

14 EXTERNAL FLOW

- 14.1 Introduction
 - 14.2 Boundary Layers: Basic Concepts
 - 14.2.1 Laminar Boundary Layer on a Flat Plate
 - 14.2.2 Turbulent Boundary Layer on a Flat Plate
 - 14.2.3 Boundary Layer on an Airfoil or Other Body
 - 14.3 Drag: Basic Concepts
 - 14.4 Drag Coefficients
 - 14.4.1 Low Reynolds Number Flow
 - 14.4.2 Cylinders
 - 14.4.3 Spheres
 - 14.4.4 Bluff Bodies
 - 14.5 Lift and Drag of Airfoils
 - 14.6 Summary
 - Problems

14.1 INTRODUCTION

An external flow occurs whenever an object moves through a fluid or a fluid passes by the surface of a structure. Such flows are present everywhere in the world around us, both in nature and as a result of modern technology. Nearly all living creatures, from the smallest bacterium to the largest mammal, encounter air or water in motion. In fact, some animals, such as pelicans and other diving birds, are equipped to deal with locomotion in both fluids. Humans have often looked to the animal world for inspiration in their desire for enhanced mobility on land, sea, and air. Despite some success in simply copying natural designs, the development of aircraft, ships, and to a lesser extent, land vehicles such as automobiles could not have occurred without a good understanding of external flow. Today, in technical problems ranging from how particles settle onto the surface of the lung to the effects of wind blowing over a building, understanding the interaction between an object moving through a fluid (or equivalently fluid moving over an object or adjacent to a structure), remains of great practical importance.

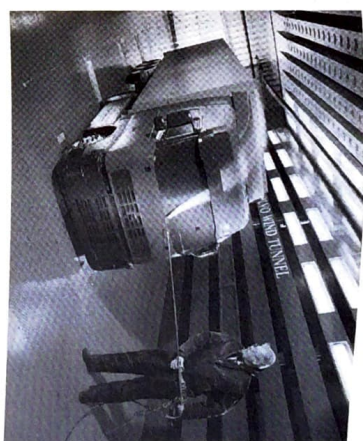


Figure 14.1 Aerodynamic testing of a truck with smoke in a wind tunnel.

CD/Video library/Butterflies & Flow past a larvae & Gold fish & Pine cone & Pine needles & Sperrn

Some aspects of external flow have been mentioned in earlier chapters, both because they are fundamentally useful in engineering design and to provide a foundation for this chapter. Before continuing you may find it helpful to revisit the case studies in Sections 3.3.4 (flat plate boundary layer), 3.3.5 (drag on cylinders and spheres), and 3.3.6 (lift and drag on airfoils), as well as those dealing with fluid force exerted on a body in an external flow in Sections 4.5.1 (flow over a flat plate), and 4.5.3 (lift and drag). An experienced engineer can often obtain a good feel for the forces generated by external flows by using flow visualization. Thus you may also wish to review the flow visualization concepts in Chapter 10. Have you seen commercials featuring a car or other vehicle in a wind tunnel with streamlines of smoke passing over the surface, as shown in Figure 14.1? The streamlines reveal regions of flow separation that contribute to drag. A number of other things you have learned are also relevant to your study of external flow. Examples include the analytical and computational fluid dynamics solutions for flow over a cylinder presented in Chapter 12, and the brief discussion of turbulence in that same chapter. As you will learn, turbulence plays a critical role in external flow. The presence or absence of turbulence strongly influences boundary layer development, flow separation, and the forces exerted by a fluid on an immersed object.

CD/Video library/Flow past cars

Our discussion of external flow begins with the concept of a boundary layer, a thin layer of moving fluid near a solid surface in which the no-slip condition and viscosity combine to create a velocity gradient. That velocity gradient creates a shear stress on the adjacent surface in the direction of the nearby flow. Since the flow in a boundary layer can be laminar or turbulent, we will discuss the characteristics of each type, limiting ourselves at first to the simplest case of flow along a flat plate. We next briefly discuss the boundary layer on airfoils and other objects for which the curvature of the surface and angle of incidence of the freestream are important. We conclude the chapter with

sections devoted to the discussion of drag coefficients, and lift and drag of airfoils. Many of the results in these sections are based on empirical observations that have been collapsed by dimensional analysis into lists of the familiar lift and drag coefficients introduced in the case studies. Examples of the use of those coefficients in solving a variety of external flow problems are provided. Throughout this chapter you will also find a qualitative discussion of how lift and drag are generated by the flow field. We include this discussion to help you understand how changes in the flow field about an immersed body can have dramatic effects on the force applied to the body by the fluid.

CD/Boundary layers/Boundary layer concepts

14.2 BOUNDARY LAYERS: BASIC CONCEPTS

When a body is immersed in a moving fluid, the fluid velocity along a line perpendicular to any point on the body surface is observed to vary from zero on the surface to a maximum value some distance away. At small Reynolds numbers, the distance over which the velocity variation occurs may be of the same magnitude as the dimensions of the body itself. However, at large Re the variation occurs over a relatively small distance, and the body is said to have a boundary layer, meaning that there is a layer of fluid near the surface of the body in which the velocity changes from zero on the surface to the freestream value. Prandtl's insight into this phenomenon and his subsequent development of boundary layer theory are milestones in the development of fluid mechanics.

The characteristics of a boundary layer are affected by the shape of the solid surface of interest, the orientation of the surface relative to the freestream, and many other factors. However, we can illustrate the basic concepts by examining the boundary layer on a thin flat plate aligned with the freestream. Consider the boundary layer on the upper surface of such a plate at large Reynolds number as shown in Figure 14.2. The flow is steady, and we can define a Reynolds number for the flow by using the length L of the plate and freestream velocity U to write $Re_L = UL/\nu$. In a fluid of relatively small kinematic viscosity such as air or water, the requirement of a large Reynolds number means that the freestream velocity U is large. Observation shows that at large Reynolds

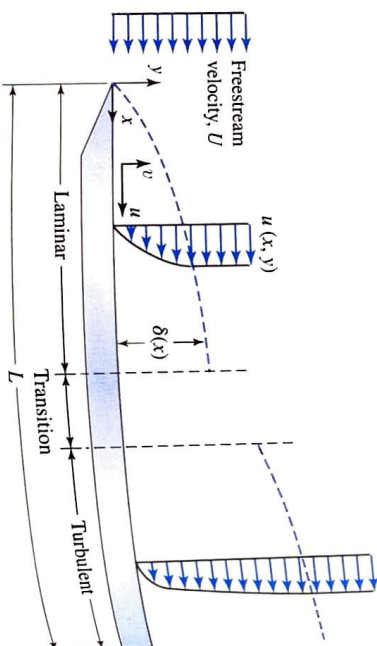


Figure 14.2 Geometry for flow over a flat plate.

numbers the boundary layer is relatively thin, and the thickness of the boundary layer increases in the downstream direction. Moreover, just downstream of the nose of the plate the boundary layer is observed to be laminar, but at some point downstream transition occurs and the boundary layer becomes turbulent.

At any location x along the plate, there is a smooth variation in the streamwise velocity component u along a line perpendicular to the plate surface. Thus, u is a function of x and y inside the boundary layer, but a constant U outside. The transverse velocity component, v , is also observed to be a function of x and y inside the boundary layer, but it is zero outside. The transverse velocity component v in a boundary layer is very small compared to u . Thus one boundary layer characteristic is $v \ll u$. A second characteristic is based on the observation that the velocity changes rapidly in a direction normal to the surface, but slowly in the flow direction. This means that spatial derivatives of the velocity in the flow direction inside the boundary layer are small in comparison to spatial derivatives in the normal direction.

The approach of the streamwise velocity component u to the freestream value is asymptotic. Nevertheless, we can define a boundary layer thickness δ as the height above the plate at which $u = 0.99 U$, meaning that the streamwise velocity component is within one percent of the freestream value. Observation shows that the boundary layer thickness grows at one rate in the laminar region, another rate in the transition region, and yet another rate in the turbulent region. Since the thickness of a boundary layer depends on the location x along the plate, we write $\delta = \delta(x)$ and recognize that this function is an important characteristic of a boundary layer, since it defines the edge where the boundary layer and freestream meet. Note that this edge (dashed line in Figure 14.2) is not a streamline. In fact, streamlines enter the boundary layer all along its length.

It is customary to define two additional quantities that also characterize the thickness of a boundary layer. The first of these, called the displacement thickness and represented by δ^* , is defined by the following integral

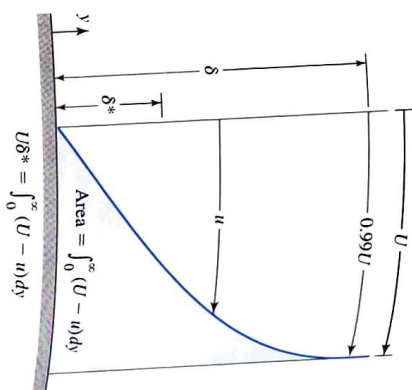
$$\delta^* = \int_0^\infty \left(1 - \frac{u}{U}\right) dy \quad (14.1)$$

This integral takes a different value at each location x along the plate, so we write $\delta^* = \delta^*(x)$. One rationale for defining the displacement thickness in this way is illustrated in Figure 14.3, where we have overlaid the velocity profile in the boundary layer on top of the uniform velocity profile that would exist if the fluid were inviscid and able to slip by the plate. The shaded area can be thought of as the volume flowrate per unit width w into the paper that is missing because of the presence of the boundary layer. The difference in volume flowrate carried by the two velocity profiles is seen to be given by $\Delta Q = w \int_0^\infty U dy - w \int_0^\infty u dy$. With a little rearrangement we can write this as

$$\Delta Q = w \int_0^\infty (U - u) dy = wU \int_0^\infty \left(1 - \frac{u}{U}\right) dy = U w \delta^*$$

Thus the missing volume flowrate in the boundary layer is seen to be given by $\Delta Q = U w \delta^*$, and the missing mass flowrate is $\Delta \dot{M} = \rho U w \delta^*$. From this analysis, and recalling that the passage formed by two adjacent streamlines carries a certain volume flowrate in proportion to their distance apart, it is customary to say that in comparison to a fictitious inviscid flow over the plate, a boundary layer displaces streamlines a distance

Figure 14.3 Definitions of boundary layer and displacement thickness.



δ^* away owing to viscous effects. Another way of describing δ^* is to say that the boundary layer makes a body appear δ^* thicker owing to the effects of viscosity in slowing down fluid near the body surface. That is, the body surface is effectively defined by the edge of the boundary layer.

The second additional quantity that is used to characterize the thickness of a boundary layer is $\Theta = \Theta(x)$, called the momentum thickness. The momentum thickness is defined by

$$\Theta = \int_0^\infty \frac{u}{U} \left(1 - \frac{u}{U}\right) dy \quad (14.2)$$

A streamwise momentum balance can be used to show that in comparison to an inviscid flow, the missing streamwise momentum flux in the boundary layer is equal to $\rho U^2 w \Theta$. Each of the three thicknesses, $\delta = \delta(x)$, $\delta^* = \delta^*(x)$, and $\Theta = \Theta(x)$ plays an important role in discussions of boundary layers.

Additional quantities of importance in boundary layer theory are the wall shear stress, $\tau_w = \tau_w(x)$, which is a function of position along the plate because of the changing streamwise velocity profile, and the total force exerted by the fluid on the plate.

The total force on the plate can be thought of as consisting of lift and drag. The lift component of this force is defined by Eq. 4.25b as $F_L = \int_S (-p \mathbf{n} + \boldsymbol{\tau}) \cdot \mathbf{n}_L dS$, where the unit vector \mathbf{n}_L is normal to the plate. For a flat plate aligned with the freestream, the wall shear stress acts along the plate, i.e., in the streamwise direction, so there can be no contribution to lift from the shear stress. In addition, the symmetry of the flow ensures that the pressure distribution on both sides of the plate is the same. Thus the lift is zero and the total force on a flat plate aligned with the freestream consists solely of drag. The drag force on the plate is defined by Eq. 4.26b as $F_D = \int_S (-p \mathbf{n} + \boldsymbol{\tau}) \cdot \mathbf{n}_D dS$, where the unit vector \mathbf{n}_D points in the flow direction. Since the pressure acts normal to the plate, it cannot contribute to the drag, and the drag on each side of a plate of width w and length L is given by

$$F_D = w \int_0^L \tau_w(x) dx \quad (14.3)$$

From this we see that the wall shear stress distribution is indeed of great interest in boundary layer analysis.

At this point we can begin to investigate the relationships among these boundary layer parameters by employing dimensional analysis. In doing DA on this problem, it is customary to choose the spatial coordinate x as the length scale, rather than the length of the plate L . The DA is otherwise routine and yields the following relationships:

$$\frac{\delta}{x} = f_1 \left(\frac{Ux}{\nu} \right) = f_1(Re_x) \quad (14.4)$$

$$\frac{\tau_w}{\rho U^2} = f_2 \left(\frac{Ux}{\nu} \right) = f_2(Re_x) \quad (14.5)$$

where the Reynolds number based on x is given by

$$Re_x = \frac{Ux}{\nu} \quad (14.6)$$

Introducing the skin friction coefficient $C_f = \tau_w / \frac{1}{2} \rho U^2$, we can write Eq. 14.5 as

$$C_f = f_3 \left(\frac{Ux}{\nu} \right) = f_3(Re_x) \quad (14.7)$$

DA alone cannot tell us the form of these unknown relationships, but as shown in the next two sections, theory and empirical data can.

14.2.1 Laminar Boundary Layer on a Flat Plate

H. Blasius, one of Prandtl's students, analyzed the steady, laminar boundary layer on a smooth flat plate aligned with the freestream in 1908. We can derive his result, known as the Blasius solution, by using Cartesian coordinates with the plate aligned with the x axis as shown in Figure 14.4. In general, the equations of motion for a steady, constant density, constant viscosity flow are given by Eqs. 12.1a–12.1d. However, there is no reason to expect a cross-stream velocity component w in the flow over a flat plate, nor any variation of a flow property in the z direction. Thus the flow is 2D. Inserting $w = 0$, and

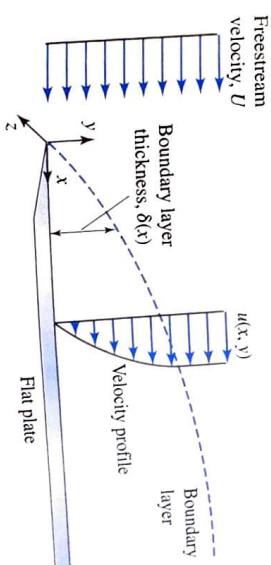


Figure 14.4 The geometry of the boundary layer over a flat plate.

HISTORY BOX 14-1

Heinrich Blasius is famous in fluid mechanics for his boundary layer solution and other contributions he made while studying under Prandtl. However, later in life he left fluid mechanics research to teach at a Hamburg engineering school.

dropping all derivatives with respect to z in Eqs. 12.1a–12.1d, yields the following equations as the starting point for a discussion of the flat plate boundary layer:

$$\frac{\partial u}{\partial x} + \frac{\partial v}{\partial y} = 0$$

$$\rho \left(u \frac{\partial u}{\partial x} + v \frac{\partial u}{\partial y} \right) = -\frac{\partial p}{\partial x} + \mu \left(\frac{\partial^2 u}{\partial x^2} + \frac{\partial^2 u}{\partial y^2} \right)$$

$$\rho \left(u \frac{\partial v}{\partial x} + v \frac{\partial v}{\partial y} \right) = -\frac{\partial p}{\partial y} + \mu \left(\frac{\partial^2 v}{\partial x^2} + \frac{\partial^2 v}{\partial y^2} \right)$$

CD/Boundary layers/Laminar boundary layers

Further simplification of these equations can be made by recalling that the flow in a boundary layer is predominantly parallel to the surface on which it occurs. Thus we can assume $v \ll u$. Furthermore, the boundary layer is thin, which implies that derivatives of flow variables with respect to x are much smaller than those with respect to y . By using these two assumptions to simplify the preceding set of equations, we obtain

$$\frac{\partial u}{\partial x} + \frac{\partial v}{\partial y} = 0 \quad (14.8a)$$

$$\rho \left(u \frac{\partial u}{\partial x} + v \frac{\partial u}{\partial y} \right) = -\frac{\partial p}{\partial x} + \mu \left(\frac{\partial^2 u}{\partial y^2} \right) \quad (14.8b)$$

$$0 = -\frac{\partial p}{\partial y} \quad (14.8c)$$

These are the Prandtl boundary layer equations. They can be shown to be applicable to boundary layers on moderately curved as well as flat surfaces, an important point to keep in mind throughout the rest of our discussion.

Before we worry about solving these equations, notice that the last equation tells us that the pressure in the boundary layer does not vary across the boundary layer. Thus we conclude that the pressure inside the boundary layer on flat and moderately curved surfaces is the same as it is in the inviscid flow outside the boundary layer. This is a very important aspect of Prandtl's boundary layer equations, for it shows that finding the gradient in Eq. 14.8b may be considered to be known and determined by finding the pressure distribution in the inviscid flow over the same surface shape.

Blasius was able to solve the Prandtl boundary layer equations for a flat plate by recognizing that since the pressure in an inviscid flow over a flat plate is uniform, the pressure gradient $\partial p / \partial x$ in Eq. 14.8b is zero. Thus the flat plate boundary layer is

described by:

$$\frac{\partial u}{\partial x} + \frac{\partial v}{\partial y} = 0 \quad (14.9a)$$

$$\rho \left(u \frac{\partial u}{\partial x} + v \frac{\partial u}{\partial y} \right) = \mu \left(\frac{\partial^2 u}{\partial y^2} \right) \quad (14.9b)$$

These two equations, with the associated boundary conditions, must be solved for the unknown velocity components. The no-slip, no-penetration boundary conditions that describe the flow over a flat plate are $u(x, 0) = 0$ and $v(x, 0) = 0$ for $x > 0$. We also want the boundary layer solution to match the inviscid freestream solution $u = U$ that exists upstream of the plate and above the plate outside the boundary layer. These last two conditions can be written as $u \rightarrow U$, $v \rightarrow 0$ for $x < 0$, and $u \rightarrow U$, $v \rightarrow 0$ for $y \gg \delta$, i.e., outside the boundary layer. Here U is the magnitude of the freestream velocity.

Although there is no known solution to Eqs. 14.9a and 14.9b that satisfies these conditions exactly, Blasius showed that a similarity solution of these equations can be obtained by introducing a new variable

$$\eta = \left(\frac{U}{\nu x} \right)^{1/2} y \quad (14.10a)$$

and employing a streamfunction

$$\psi(x, y) = (U\nu x)^{1/2} f(\eta) \quad (14.10b)$$

The word “similarity” used to describe this solution indicates that when properly scaled in the similarity variable, $\eta = (U/\nu x)^{1/2} y$, the velocity profiles at every location along the flat plate collapse onto a single universal curve. Thus the profiles are similar.

Now by the definition of a streamfunction we have $u = \partial\psi/\partial y$ and $v = -\partial\psi/\partial x$, thus Eq. 14.9a is automatically satisfied. The velocity components are found to be given by

$$u = \frac{\partial}{\partial y} [(U\nu x)^{1/2} f(\eta)] = \frac{\partial f}{\partial \eta} \frac{\partial \eta}{\partial y} = U \frac{\partial f}{\partial \eta}$$

and

$$v = -\frac{\partial \psi}{\partial x} = -\frac{\partial}{\partial x} [(U\nu x)^{1/2} f(\eta)] = \left(\frac{U\nu}{4x} \right)^{1/2} \left(\eta \frac{\partial f}{\partial \eta} - f \right)$$

Substituting these velocity components into Eq. 14.9b, simplifying, and making the key similarity assumption that the function f is not separately a function of x , we obtain the following nonlinear, third-order, ordinary differential equation:

$$\frac{d^3 f}{d\eta^3} + f \frac{df}{d\eta} = 0 \quad (14.11)$$

TABLE 14.1 Blasius Solution

η	f	$\frac{\partial f}{\partial \eta}$	$\frac{\partial^2 f}{\partial \eta^2}$
0	0	0	0
0.5	0.0415	0.1659	0.3321
1.0	0.1656	0.3298	0.3309
1.5	0.3701	0.4868	0.3230
2.0	0.6500	0.6298	0.3026
2.5	0.9963	0.7513	0.2668
3.0	1.3968	0.8460	0.2174
3.5	1.8377	0.9130	0.1614
4.0	2.3057	0.9555	0.1078
4.5	2.7901	0.9795	0.0642
5.0	3.2833	0.9915	0.0340
5.5	3.7806	0.9969	0.0159
6.0	4.2796	0.9990	0.0066
6.5	4.7793	0.9997	0.0024
7.0	5.2792	0.9999	0.0008
7.5	5.7792	1.0000	0.0001
8.0	6.2792	1.0000	0.0000

The boundary conditions for this equation are $f = df/d\eta = 0$ at $\eta = 0$, and $df/d\eta \rightarrow 1$ as $\eta \rightarrow \infty$.

The function $f(\eta)$ that satisfies this equation and boundary conditions defines the Blasius solution. This function must be obtained numerically. Table 14.1 contains values of f , $df/d\eta$, and $d^2f/d\eta^2$. These are readily found by using Mathematica or another symbolic code to solve the differential equation. Notice that the edge of the boundary layer, defined as the location at which $df/d\eta = u/U = 0.99$, occurs at $\eta \approx 5.0$.

CD/Special features/Virtual labs/Blasius Boundary Layer Growth

The streamwise velocity profiles at various locations, shown in Figure 14.5A, exhibit the growth in the thickness of the boundary layer at locations away from the nose of the plate. When properly scaled in the similarity variable, all the profiles in Figure 14.5A collapse onto a single universal curve: the boundary layer velocity profile $u/U = df/d\eta$ as shown in Figure 14.5B. We see the expected boundary layer behavior: a zero velocity on the wall with a gradual approach to the freestream value near $\eta = 5.0$.

Because the governing equations have been simplified to derive the Blasius solution, it is necessary to confirm experimentally that the velocity profiles in the flat plate boundary layer do exhibit similarity. Figure 14.6A shows the similar profiles in the laminar flow region beginning just downstream of the nose of the plate. In the bottom left

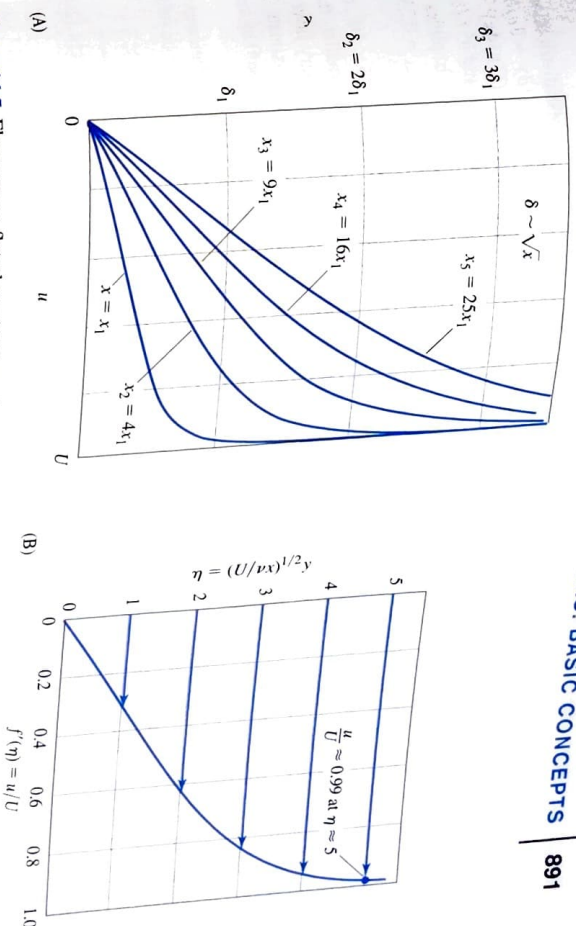


Figure 14.5 Flow over a flat plate: (A) boundary layer velocity profiles along the plate and (B) the equivalent similarity profile.

corner of Figure 14.6B the laminar profile is also present. But after the onset of turbulence the velocity profiles are no longer similar. Thus the Blasius similarity solution, which is valid for the laminar flow boundary layer, confirmed Prandtl's basic ideas about the boundary layer.

CD/Demonstrations/Blasius and Falkner-Skan solutions

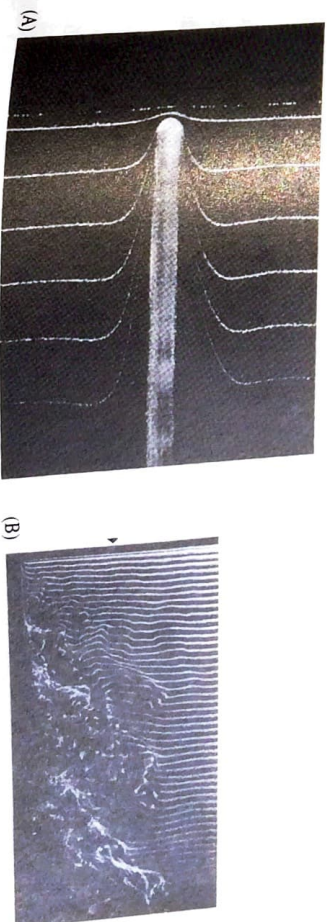


Figure 14.6 Flow visualization of flow over a flat plate using hydrogen bubbles to create material lines. (A) Laminar boundary layer near the nose of the plate, and (B) A wider view showing the transition into a turbulent boundary layer.

The Blasius solution also provides information about the shear stress distribution on the plate. The shear stress is given by Eq. 11.6d as $\sigma_{xy} = \sigma_{yx} = \mu(\partial u/\partial y + \partial v/\partial x)$. Evaluating this expression by using $u = U(\partial f/\partial \eta)$ and $v = (U\nu/4x)^{1/2} \times [\eta(\partial f/\partial \eta) - f]$ results in a complicated expression involving f , $\partial f/\partial \eta$, and $\partial^2 f/\partial \eta^2$. However, at the wall $y = 0$, the expression for the shear stress simplifies to $\sigma_{xy} = \sigma_{yx} = \mu U \sqrt{U/\nu x} (\partial^2 f/\partial \eta^2)|_{y=0}$, so only the value $(\partial^2 f/\partial \eta^2)|_{y=0} = 0.3321$ is needed to calculate τ_w .

Since transition to a turbulent boundary is observed at roughly $Re_x \approx 5 \times 10^5$, the Blasius solution is valid for a value of x greater than zero but smaller than $x \approx 5 \times 10^5(\nu/U)$. However, the precise location of transition in a boundary layer is not as certain as this appears to indicate. Thus this range of validity is approximate. In fact it is possible to force the transition to a turbulent boundary layer near $x = 0$ by various means, including a trip wire or artificial roughness.

Within these constraints, the laminar flat plate boundary problem may be considered solved. The quantities of interest calculated from the Blasius solution may be summarized as follows:

$$Re_x = \frac{Ux}{\nu} \quad (14.12a)$$

$$\frac{\delta(x)}{x} = 5.0(Re_x)^{-1/2} \quad (14.12b)$$

$$\frac{\delta^*(x)}{x} = 1.721(Re_x)^{-1/2} \quad (14.12c)$$

$$\frac{\Theta(x)}{x} = 0.664(Re_x)^{-1/2} \quad (14.12d)$$

$$\tau_w(x) = 0.332\rho U^2(Re_x)^{-1/2} \quad (14.12e)$$

$$C_f(x) = 0.664(Re_x)^{-1/2} \quad (14.12f)$$

By comparing these results and those obtained by DA in the Section 14.2 (Eqs. 14.4–14.7), we can see that the Blasius solution provides the unknown functional dependence on Re_x . In addition, it is evident that the similarity of the Blasius solution justifies the use of x as the length scale in the dimensional analysis. The important characteristics of the laminar flat plate boundary layer are found in Eqs. 14.12: the boundary layer thickness grows at a rate $\delta(x) \propto x^{1/2}$, and this is also true of the displacement and momentum thicknesses; the wall shear stress decreases at a rate $\tau_w(x) \propto x^{-1/2}$, as does the skin friction coefficient.

It is possible to define a drag coefficient for a flat plate. Consider the drag contributed by the boundary layer on one side of a plate of width w and length L . Inserting Eq. 14.12e into the equation defining the drag force, Eq. 14.3, and substituting $Re_x = Ux/\nu$, we obtain

$$F_D = w \int_0^L \tau_w(x) dx = w \int_0^L 0.332\rho U^2 \left(\frac{Ux}{\nu} \right)^{-1/2} dx$$

Completing the integration we find

$$F_D = \frac{0.664\rho U^2 w L}{\sqrt{Re_L}} \quad (14.12g)$$

which corresponds to a drag coefficient based on the plate area wL of

$$C_D = \frac{1.328}{\sqrt{Re_L}} \quad (14.12h)$$

Although some of these results appeared in Section 3.3.4, the example that follows further illustrates the characteristics of a laminar flat plate boundary layer.

EXAMPLE 14.1

A thin flat plate, 10 ft tall and 1 ft wide, forms the leading edge of a banner towed by an aircraft at 100 mph on a 70°F day. How far from the leading edge of the plate does the laminar portion of boundary layer extend? What is the boundary layer thickness at the downstream end of the laminar boundary layer? Find the drag force on the plate contributed by the laminar boundary layer, and the corresponding drag coefficient.

SOLUTION

The physical arrangement is shown in Figure 14.7. A laminar boundary layer is expected to transition at $Re_x \leq 5 \times 10^5$. Thus we can solve for the distance x_C to the transition point by using Eq. 14.12a to write: $x_C = (5 \times 10^5 \nu)/U$. Using $U = 100$ mph = 146.7 ft/s and, from Appendix A, $\nu = 1.64 \times 10^{-4}$ ft²/s for air, we find

$$x_C = \frac{5 \times 10^5 [1.64 \times 10^{-4} (\text{ft}^2/\text{s})]}{146.7 \text{ ft/s}} = 0.56 \text{ ft}$$

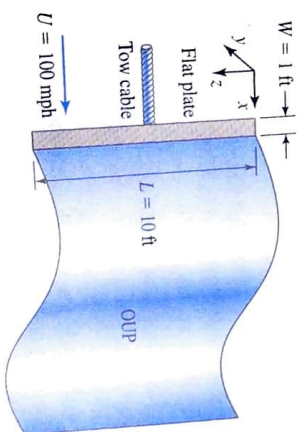


Figure 14.7 Schematic for Example 14.1.

Transition begins to occur just beyond the midpoint of the plate, and the rear portion of the plate has a turbulent boundary layer. To find the laminar boundary layer thickness at $x = x_C$ we use Eq. 14.12b to calculate the thickness as

$$\delta(x_C) = 5.0x_C(Re_x)^{-1/2} = 5.0(0.56 \text{ ft})(5 \times 10^5)^{-1/2} = 0.00396 \text{ ft} = 0.048 \text{ in.}$$

Thus the laminar boundary layer is only 0.048 in. thick when transition occurs. To find the drag force on both sides of the plate due to the laminar boundary layer, we must multiply Eq. 14.12g, which gives the drag on one side, by 2 and obtain $F_D = 1.328\rho U^2 wL/\sqrt{Re_L}$. In this case, we must also be careful to insert $L = x_C$, since this defines the portion of the plate covered by the laminar boundary layer. Using $\rho = 2.329 \times 10^{-3} \text{ slug/ft}^3$ from Appendix A, inserting the other data, and noting that $Re_L = 5 \times 10^5$, we obtain

$$\begin{aligned} F_D &= \frac{1.328\rho U^2 wL}{\sqrt{Re_L}} \\ &= \frac{1.328}{\sqrt{5 \times 10^5}} (2.329 \times 10^{-3} \text{ slug/ft}^3)(146.7 \text{ ft/s}^2)(10 \text{ ft})(0.56 \text{ ft}) = 0.53 \text{ lb}_f \end{aligned}$$

The total drag on the plate is actually much larger than this since we have not accounted for the drag of the turbulent boundary layer. The drag coefficient for the laminar portion of the boundary layer, which refers to one side of the plate only, is given by Eq. 14.12h as $C_D = 1.328/\sqrt{Re_L} = 0.0019$.

CD/Boundary layers/instability, transition, and turbulence

14.2.2 Turbulent Boundary Layer on a Flat Plate

There is no analytical solution available for a turbulent boundary layer on a smooth flat plate, so we are forced in this case to rely on empirical observations. It is customary to model the streamwise velocity profile in the turbulent boundary layer for $0 < y/\delta \leq 1$, by the power law

$$\frac{u}{U} = \left(\frac{y}{\delta}\right)^{1/7} \quad (14.13)$$

with $u = U$ for $y/\delta > 1$. Since the flow is turbulent, u is the average velocity. The boundary layer thickness is a function of x as usual, hence $\delta = \delta(x)$ and must also be determined. Figure 14.8 compares the turbulent velocity profile with the laminar profile. Note that the turbulent profile is fuller and the velocity gradient at the wall is larger than in a laminar flow. The increased mixing due to the turbulence results in a higher streamwise velocity at any given distance from the wall in comparison to the laminar profile.

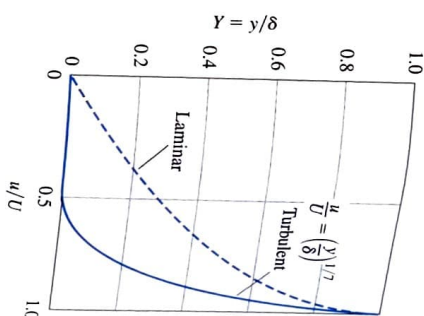


Figure 14.8 Comparison of the flat plate laminar and turbulent boundary layers.

We cannot compute a wall shear stress in turbulent flow because the constitutive relationship between shear stress and average velocity in a turbulent flow is unknown. Instead, we make use of the following empirical result for the wall shear stress

$$\tau_w(x) = 0.0225\rho U^2 \left(\frac{u}{U\delta}\right)^{1/4} \quad (14.14a)$$

This allows us to write the skin friction coefficient as

$$C_f(x) = 0.045 \left(\frac{u}{U\delta}\right)^{1/4} \quad (14.14b)$$

However, neither formula is useful as is because we do not know the boundary layer thickness $\delta = \delta(x)$. A clever solution to this dilemma consists of making use of a streamwise momentum balance on the boundary layer. Without going into the details here, if the power law given by Eq. 14.13 and the shear stress given by Eq. 14.14a are inserted into the streamwise momentum balance, the following boundary layer thickness is found:

$$\delta(x) = 0.370 \left(\frac{u}{U}\right)^{4/5} x^{4/5} \quad (14.15)$$

Comparing this to the corresponding laminar result, Eq. 14.12b, we see that the thickness of the laminar layer grows at the rate $\delta(x) \propto x^{1/2}$, while the turbulent boundary layer grows at the faster rate $\delta(x) \propto x^{4/5}$.

We can now use Eq. 14.15 to evaluate the wall shear stress, and since the velocity profile is known, we can also compute the displacement and momentum thicknesses for the turbulent boundary layer. The important characteristics of a turbulent boundary layer on a flat plate predicted by the power-law velocity profile model are summarized as follows:

$$Re_x = \frac{Ux}{\nu} \quad (14.16a)$$

$$\frac{\delta(x)}{x} = 0.370(Re_x)^{-1/5} \quad (14.16b)$$

$$\frac{\delta^*(x)}{x} = 0.0463(Re_x)^{-1/5} \quad (14.16c)$$

$$\frac{\theta(x)}{x} = 0.0360(Re_x)^{-1/5} \quad (14.16d)$$

$$\tau_w(x) = 0.0288\rho U^2(Re_x)^{-1/5} \quad (14.16e)$$

$$C_f(x) = 0.0577(Re_x)^{-1/5} \quad (14.16f)$$

$$F_D = 0.036\rho U^2 w L(Re_L)^{-1/5} \quad (14.16g)$$

$$C_D = 0.072(Re_L)^{-1/5} \quad (14.16h)$$

These results are known to be accurate for Reynolds numbers in the range $5 \times 10^5 < Re_x < 10^7$. We see that in the turbulent flat plate boundary layer, the displacement and momentum thicknesses also grow at a rate proportional to $x^{4/5}$. The wall shear stress decreases at a rate $\tau_w(x) \propto x^{-1/5}$, as does the skin friction coefficient.

Note that a power-law model for the turbulent boundary layer on a flat plate is not the only possible choice. Another model, based on a logarithmic velocity profile, is said to offer the advantage of providing accurate results for the much wider range $10^5 < Re_x < 10^9$. The boundary layer characteristics of this model are:

$$\frac{\delta(x)}{x} = 0.14(Re_x)^{-1/7} \quad (14.17a)$$

$$\tau_w(x) = 0.0125\rho U^2(Re_x)^{-1/7} \quad (14.17b)$$

$$C_f(x) = 0.025(Re_x)^{-1/7} \quad (14.17c)$$

$$F_D = 0.015\rho U^2 w L(Re_L)^{-1/7} \quad (14.17d)$$

$$C_D = 0.030(Re_L)^{-1/7} \quad (14.17e)$$

EXAMPLE 14.2

A box-shaped truck body 2.5 m wide, 3 m high, and 7 m long (Figure 14.9) is traveling at 20 m/s in 20°C air. Calculate the contributions to the total drag of the truck from the sides and top of the truck body. Assume that a sheet metal seam near the leading edge of each panel causes the boundary layer to be turbulent for the full length of the panel. Also find the wall shear stress and boundary layer thickness along the top panel, and the maximum value of the wall shear stress and boundary layer thickness on this panel.

SOLUTION

We will first use Eq. 14.16a to calculate the maximum Reynolds number at the downstream edge $x = L$ of each panel. With viscosity data from Appendix A, we obtain

$$Re_L = \frac{UL}{\nu} = \frac{(20 \text{ m/s})(7 \text{ m})}{1.51 \times 10^{-5} \text{ m}^2/\text{s}} = 9.3 \times 10^6$$

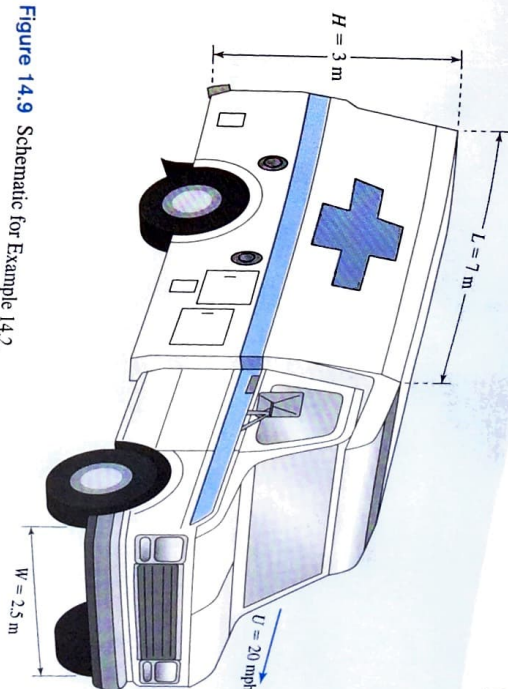


Figure 14.9 Schematic for Example 14.2.

This is just within the applicable range of Eqs. 14.16a–14.16h. The drag force on each panel is calculated by using Eq. 14.16g. For the top we obtain

$$\begin{aligned} F_{D_{\text{top}}} &= 0.036\rho U^2 w L(Re_L)^{-1/5} \\ &= \frac{0.036(1.204 \text{ kg/m}^3)(20 \text{ m/s})^2(2.5 \text{ m})(7 \text{ m})}{(9.3 \times 10^6)^{1/5}} \\ &= 12.3 \text{ N} \end{aligned}$$

The drag on each side panel is found using the same formula with $w = 3 \text{ m}$ instead of $w = 2.5 \text{ m}$. Thus we can write $F_{D_{\text{side}}} = (3/2.5)F_{D_{\text{top}}} = 14.8 \text{ N}$. The drag of all three panels is now calculated as $F_D = 2F_{D_{\text{side}}} + F_{D_{\text{top}}} = 2(14.8 \text{ N}) + 12.3 \text{ N} = 41.9 \text{ N}$. To find the boundary layer thickness and wall shear stress on the top panel, we use Eqs. 14.16b and 14.16e, respectively. Writing these explicitly in terms of x we have

$$\delta^*(x) = 0.370x \left(\frac{Ux}{\nu} \right)^{-1/5} = 0.370 \left(\frac{20 \text{ m/s}}{1.51 \times 10^{-5} \text{ m}^2/\text{s}} \right)^{-1/5} x^{4/5} = 0.022x^{4/5} \text{ m}^{1/5}$$

$$\begin{aligned} \tau_w(x) &= 0.0288\rho U^2 \left(\frac{Ux}{\nu} \right)^{-1/5} \\ &= 0.0288(1.204 \text{ kg/m}^3)(20 \text{ m/s})^2 \left(\frac{20 \text{ m/s}}{1.51 \times 10^{-5} \text{ m}^2/\text{s}} \right)^{-1/5} x^{-1/5} \\ &= 0.83x^{-1/5} (\text{N/m}^2)(\text{m}^{1/5}) \end{aligned}$$

Note that these results for $\delta(x)$ and $\tau_w(x)$ also apply to the side panels. The maximum value of the shear stress and boundary layer thickness on each panel will occur at $x = L$. Inserting the data we find:

$$\delta(L) = 0.022L^{4/5}m^{1/5} = 0.022(7\text{ m})^{4/5}m^{1/5} = 0.104\text{ m} = 10.4\text{ cm}$$

$$\tau_w(L) = 0.83L^{-1/5}(N/m^2)(m^{1/5}) = (0.83)(7\text{ m})^{-1/5}(N/m^2)(m^{1/5}) = 0.56\text{ N/m}^2$$

We can repeat the calculations of the last problem, using the logarithmic model to define the various boundary layer characteristics. We will calculate values at $Re_L = UL/\nu = 9.3 \times 10^6$ and use Eq. 14.17d to calculate the drag, Eq. 14.17a to calculate the boundary layer thickness, and Eq. 14.17b to calculate the wall shear stress. The drag on the top panel is given by

$$F_{D_{top}} = \frac{0.015\rho U^2 WL}{(Re_L)^{1/7}} = \frac{0.015(1.204\text{ kg/m}^3)(20\text{ m/s})^2(2.5\text{ m})(7\text{ m})}{(9.3 \times 10^6)^{1/7}} = 12.8\text{ N}$$

Each side panel contributes $F_{D_{side}} = (3/2.5)F_{D_{top}} = 15.4\text{ N}$, yielding a total drag of 43.6 N. This is slightly larger than the 41.9 N drag calculated with the power-law model. For the boundary layer thickness we use Eq. 14.17a to write $\delta(x) = 0.14x(Re_x)^{-1/7}$ and, after inserting the data, we obtain $\delta(x) = 0.14x(Ux/\nu)^{-1/7} = 0.14(20\text{ m/s})(1.51 \times 10^{-5}\text{ m}^2/\text{s})^{-1/7}x^{6/7} = 0.019x^{6/7}\text{ m}^{1/7}$, which yields a thickness at $L = 7\text{ m}$ of $\delta(L) = 0.019x^{6/7}\text{ m}^{1/7} = 0.019(7\text{ m})^{6/7}\text{ m}^{1/7} = 0.1\text{ m} = 10\text{ cm}$. This is a slightly smaller value than that obtained with the power-law model. From Eq. 14.17b the wall shear stress is given by

$$\begin{aligned}\tau_w(x) &= 0.0125\rho U^2 \left(\frac{Ux}{\nu}\right)^{-1/7} = 0.0125(1.204\text{ kg/m}^3)(20\text{ m/s})^2 \left(\frac{20\text{ m/s}}{1.51 \times 10^{-5}\text{ m}^2/\text{s}}\right)^{-1/7} x^{-1/7} \\ &= 0.80x^{-1/7}(N/m^2)(m^{1/7})\end{aligned}$$

and the wall shear stress at $L = 7\text{ m}$ is found to be

$$\tau_w(L) = 0.80L^{-1/7}(N/m^2)(m^{1/7}) = 0.80(7\text{ m})^{-1/7}(N/m^2)(m^{1/7}) = 0.61\text{ N/m}^2$$

which is slightly larger than that calculated with the power-law model. For engineering purposes these values are equivalent to those found with the power-law model.

14.2.3 Boundary Layer on an Airfoil or Other Body

Consider the high speed flow over an airfoil at a small angle of attack as shown in Figure 14.10A. The upper and lower surfaces of the airfoil are curved, and neither surface is aligned with the freestream. Thus the results obtained earlier for the boundary layer on an aligned flat plate cannot be expected to apply to the boundary layer on this airfoil or, for that matter, to other objects of finite thickness. In fact, observation of boundary layers on airfoils and other bodies show that the shape of an object and its angle of incidence to the freestream have a significant effect on the characteristics of both laminar and turbulent boundary layers. For reasons that will become clear in a moment, this effect is described as the effect of a pressure gradient on the boundary layer.

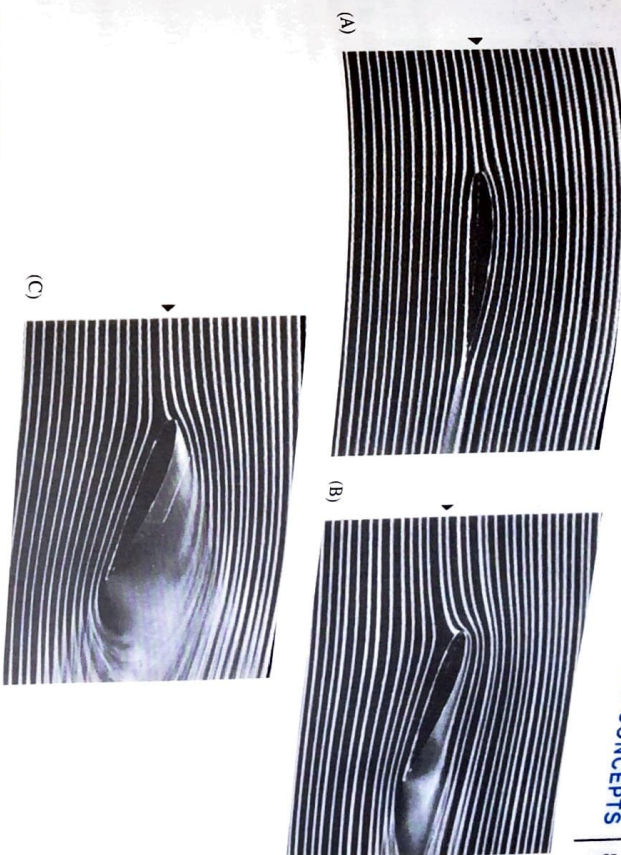


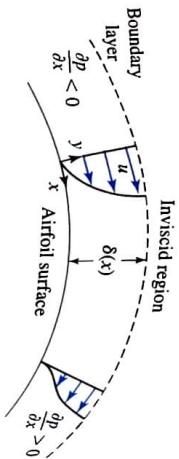
Figure 14.10 Flow around a NACA 4412 airfoil section visualized with smoke. (A) At a 2° angle of attack there is no boundary layer separation. (B) At a 15° angle of attack there is significant boundary layer separation. (C) Slightly increasing the angle of attack over 15° results in stall. In an airplane this would result in a loss of lift such that the aircraft would begin to fall.

Although a complete discussion of laminar and turbulent boundary layers on airfoils and other bodies is beyond the scope of this text, some insight into the effects of body shape and angle of incidence can be gained by considering a laminar boundary layer. Recall that a laminar boundary layer is described by the Prandtl boundary layer equations (Eqs. 14.8a–14.8c):

$$\frac{\partial u}{\partial x} + \frac{\partial v}{\partial y} = 0, \quad \rho \left(u \frac{\partial u}{\partial x} + v \frac{\partial u}{\partial y} \right) = -\frac{\partial p}{\partial x} + \mu \left(\frac{\partial^2 u}{\partial y^2} \right), \quad \text{and} \quad 0 = -\frac{\partial p}{\partial y}$$

These equations apply to the laminar boundary layer on a curved surface, provided the thickness of the boundary layer is small in comparison to the radius of curvature of the surface. It is also necessary for the boundary layer to be attached, meaning that the boundary layer must follow the contour of the surface. This is not the case if flow separation occurs. These constraints are usually met by thin airfoil shapes at a small angle of attack, as is the case in Figure 14.10B. However, if the angle of attack is increased, as shown in Figure 14.10B, the flow begins to separate, the boundary layer is not completely attached, and recirculation occurs. At higher angles of attack the airfoil is said to stall, as illustrated in Figure 14.10C. The lift of the airfoil decreases significantly when an airfoil stalls.

Figure 14.11 Boundary layer flow geometry over a curved surface.



To apply the Prandtl equations to an airfoil or other moderately curved surface, the x coordinate axis is assumed to lie along the surface and the y coordinate axis is then normal to the surface as shown in Figure 14.11. Eq. 14.8c shows that component of the pressure gradient normal to a curved surface, $\partial p / \partial y$, is negligible, just as in the case with the boundary layer on a flat plate. However, the component of the pressure gradient in the streamwise direction, $\partial p / \partial x$, which is zero for a flat plate aligned with the freestream, is nonzero on a curved surface and varies with x . Thus the boundary layer on the curved surface of a body satisfies the following equations:

$$\frac{\partial u}{\partial x} + \frac{\partial v}{\partial y} = 0 \quad (14.18a)$$

$$\rho \left(u \frac{\partial u}{\partial x} + v \frac{\partial u}{\partial y} \right) = -\frac{\partial p}{\partial x} + \mu \left(\frac{\partial^2 u}{\partial y^2} \right) \quad (14.18b)$$

The streamwise pressure gradient, which may be positive or negative, depends on the body shape and angle of incidence, as well as the location x along the body surface. To solve Eqs. 14.18a and 14.18b for the velocity components and extract the desired characteristics of the boundary layer such as its thickness and the wall shear stress, it is necessary to know the pressure gradient.

An essential part of Prandtl's boundary layer theory is the assumption that the streamwise pressure gradient $\partial p / \partial x$ is determined by the inviscid flow just outside the boundary layer. This can be explained as follows. Since the effects of viscosity are confined to the boundary layer, the flow outside is an inviscid flow. There is no pressure gradient $\partial p / \partial y$ normal to the surface in the boundary layer equations; thus the pressure distribution inside the boundary layer is the same as that just outside. Furthermore, in an unseparated flow at the high Reynolds numbers of interest, the boundary layer is very thin and may be considered in a first approximation to have vanishingly small thickness insofar as the inviscid flow is concerned. Thus in solving the inviscid flow problem, we can neglect the presence of a boundary layer and its unknown thickness and simply consider the inviscid flow over the same body at the desired freestream velocity.

After obtaining a solution for the inviscid flow, we can write the inviscid surface pressure distribution on the body using the Bernoulli equation as

$$p_S(x) + \frac{1}{2} \rho u_S(x)^2 = C \quad (14.19)$$

where $p_S(x)$ is the pressure on the surface, $u_S(x)$ is the velocity on the surface as predicted by the inviscid flow solution, and C is a constant. The pressure distribution $p_S(x)$ is assumed to be the pressure acting on the boundary layer, and we can use it to determine the streamwise pressure gradient needed to solve the boundary layer equations, writing

$$\frac{\partial p}{\partial x} = \frac{dp_S(x)}{dx} = -\frac{1}{2} \rho \frac{d}{dx} [u_S(x)^2] \quad (14.20)$$

From this discussion, we see that the effects of body shape and angle of incidence are equivalent, insofar as a boundary layer is concerned, to a streamwise pressure gradient. Thus, as mentioned earlier, it is customary to consider the effects of body shape and angle of incidence together as being equivalent to the effect of an imposed pressure gradient.

This approach allows us to understand the effects of an imposed pressure gradient, near flow: we use Eq. 14.20 to replace the pressure gradient in the boundary layer equations to obtain

$$\frac{\partial u}{\partial x} + \frac{\partial v}{\partial y} = 0$$

$$\rho \left(u \frac{\partial u}{\partial x} + v \frac{\partial u}{\partial y} \right) = \frac{1}{2} \rho \frac{d}{dx} [u_S(x)^2] + \mu \left(\frac{\partial^2 u}{\partial y^2} \right) \quad (14.21a)$$

$$(14.21b)$$

An interesting solution to these equations, called the Falkner-Skan solution, illustrates the effect of a pressure gradient on a laminar boundary layer by assuming that the surface velocity is of the form $u_S(x) = cx^m$, where c and m are constants with $c > 0$. Since $[du_S(x)]/dx = mcx^{m-1}$, the flow is accelerating for $m > 0$ and decelerating for $m < 0$. From Bernoulli's equation, we know that if the flow is accelerating for $c > 0$, is falling, and vice versa. Thus $m > 0$ implies $dp/dx < 0$, meaning that the pressure is decreasing in the flow direction. This is referred to as a favorable pressure gradient for reasons explained shortly. Similarly, $m < 0$ implies $dp/dx > 0$, which is termed an unfavorable pressure gradient. For $m = 0$, Eqs. 14.21 reduce to those describing the boundary layer on a flat plate.

Although the details of the Falkner-Skan solution are beyond the scope of this text, the qualitative results are important. The favorable pressure gradient of an accelerating freestream tends to thin a laminar boundary layer and bring higher momentum fluid nearer the surface, while the unfavorable pressure gradient of a decelerating freestream tends to do the opposite. Thus, on an airfoil or other moderately curved body, we expect where the flow is accelerating, but to become thicker and possibly to separate from portions of the surface where the flow is decelerating. The wall shear stress is zero at the point of separation, and downstream of this point the flow near the wall reverses direction. This also occurs with turbulent boundary layers, although the latter are more resistant to flow separation owing to the increased amount of higher momentum fluid near the surface associated with the more blunt turbulent velocity profile.

These observations are confirmed by flow visualization studies. To illustrate boundary layer separation, consider Figure 14.12 showing velocity profiles over an airfoil at

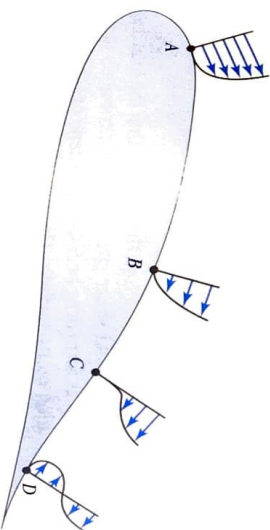
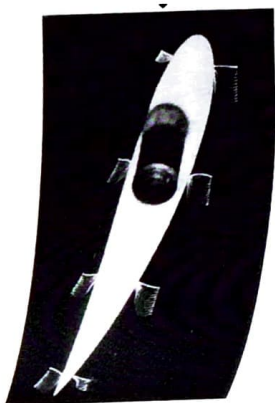


Figure 14.12 Illustration of boundary layer flow over an airfoil: A, a favorable pressure gradient; B, an unfavorable pressure gradient; C, the separation point; D, separation and flow reversal.

Figure 14.13 Flow visualization by the spark tracing method (timelines) of velocity profiles in the boundary layer.



an angle of attack. At position A, the fluid has accelerated over the front of the airfoil and the velocity profile reflects the favorable pressure gradient. At position B the effects of the unfavorable pressure gradient are apparent in that the flow has slowed in the boundary layer and the velocity profile has become steeper. At point C, the velocity profile clearly shows that $du/dy = 0$, which indicates that this is the point of separation. At position D the flow has reversed near the airfoil surface. Figure 14.13 is a flow visualization of velocity profiles in a boundary layer on an airfoil.

HISTORY BOX 14-2

The boundary layers on the airfoils of early airplanes were turbulent over much of the wing because of the presence of an unfavorable pressure gradient over 90% of that surface. Eastman Jacobs, an engineer for the National Advisory Committee on Aeronautics (NACA), designed an airfoil shape with the intent of producing a favorable pressure gradient over as much as 60% of the wing, thus maintaining laminar flow, reducing the friction drag, and increasing fuel economy. He developed the NACA-66 series of laminar flow airfoils and published his results in 1939. Those results were put to use by North American Aircraft to produce the first airplane with a laminar flow airfoil, the P-51 Mustang.

14.3 DRAG: BASIC CONCEPTS

For a stationary object immersed in a moving stream, drag is the component of force exerted on the object by the fluid in the direction of the freestream. An engineer often needs to account for the effect of drag in structural design and stability analysis, since for stationary objects ranging from buildings and trees exposed to wind to bridge piers in a river, the drag exerted by the moving fluid can be significant. For an aircraft or other object moving through a stationary fluid, the drag acts in the direction opposite to the motion of the object. The power required to propel an object through a fluid at constant speed is given by the product of drag and speed. Thus drag not only limits the performance of man-made vehicles of all types and affects the economy of operation but exerts its effects in the natural world as well.

The drag on an object is defined by Eq. 4.26b as

$$F_D = \int_S (-p\mathbf{n} + \boldsymbol{\tau}) \cdot \mathbf{n}_\infty dS$$

where the unit vector \mathbf{n}_∞ points in the flow direction. From this we see that the total drag force arises from two mechanisms: pressure and shear stress. The contribution to the total drag due to the pressure is referred to as form drag because the shape or form of the object determines the pressure distribution on its surface. The contribution to the total drag due to the shear stress acting on an object is called friction drag. In a high Reynolds

number flow, friction drag can be attributed to the boundary layer and wall shear stress as discussed earlier.

An effective way to illustrate the concepts of friction and form drag is shown in Figure 14.14. For a flat plate aligned with the freestream (Figure 14.14A), the drag is shown in Figure 14.14B, the drag is wholly due to the wall shear stress, i.e., skin friction. If the same plate is normal to the freestream (Figure 14.14C), the drag is wholly due to the pressure difference on the front and back surfaces. Note that there is a shear stress distribution on the plate in Figure 14.14B, but the effect of the shear stress cancels owing to symmetry. Even in the absence of this symmetry, the shear stress does not act in the flow direction. Even in Figure 14.14C, but at an angle of attack, the shear stress and pressure both contribute to the drag.

14.3 DRAG: BASIC CONCEPTS

903

CD/Special Features/Demonstrations/Effect of angle of attack on flow structure

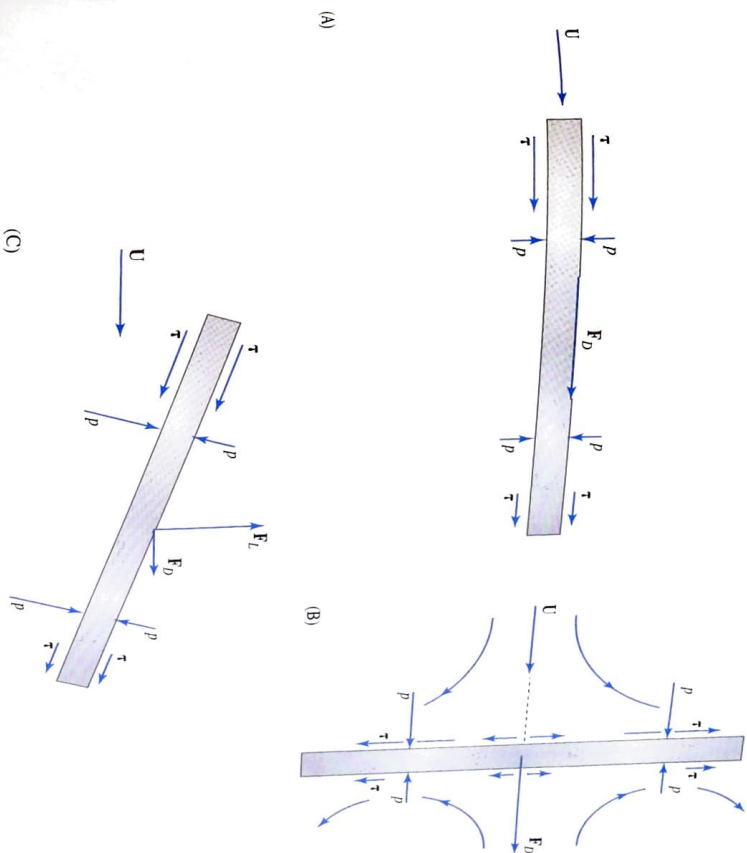


Figure 14.14 Illustration of the types of drag using flow over a flat plate: (A) aligned with the flow, friction drag only; (B) normal to the flow, form drag only; and (C) friction and form drag, present for the plate at an angle to the flow.

For any other type of body immersed in a freestream, the total drag will have contributions from both friction and form drag. Although no precise rule can be given, in a high Reynolds number flow the drag on bluff bodies, which share some of the characteristics of a flat plate held normal to the freestream, tends to be dominated by form drag. The drag on long thin bodies, like the flat plate aligned with the freestream, tends to be dominated by skin friction. "Streamlining" is a term used to describe the attempt to design an optimum shape for a bluff body in a high Reynolds number flow by minimizing the total drag. It generally takes the form of elongating the rear of the body. Although this raises the friction drag, it lowers the form drag, and the total drag is reduced. Of course, if the elongation is excessive, the friction drag eventually becomes large and the total drag is not reduced at all. The airfoil at an angle of attack described in the preceding section experiences both friction drag and form drag.

CD/Special Features/Demonstrations/Streamlining

The result of applying the concept of streamlining to a cylinder is illustrated in Figures 14.15 and 14.16. The cylinder and airfoil shape in Figure 14.15 have the same frontal area wL , but the drag on the airfoil shape is a fraction of that on the cylinder. This is emphasized in Figure 14.16, where we see a cylinder and airfoil shape having the same drag. If you are wondering about the relevance of this, early biplanes used wire cables to structurally connect the two wings, but it was eventually recognized that the drag could be lowered by using streamlined airfoil shaped struts instead of cables.

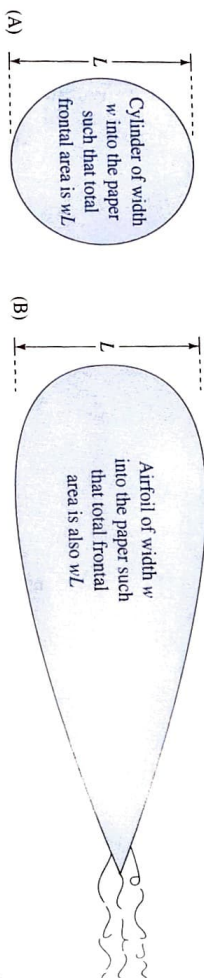


Figure 14.15 The cylinder (A) and the airfoil (B) have the same frontal area, but the drag on the cylinder is much greater.

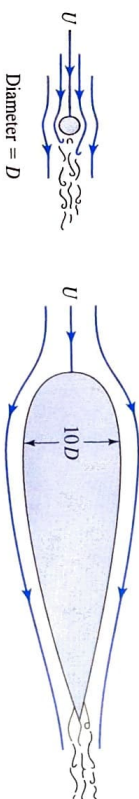


Figure 14.16 The cylinder has much less frontal area than the airfoil, yet the two shapes have the same drag.

14.4 DRAG COEFFICIENTS



Although computational fluid dynamics is increasingly being applied to the problem of determining the drag on objects of engineering interest, much of what is known about drag is the result of experiments. Suppose we apply dimensional analysis to the problem of determining the drag on an object of a specified shape and include a comprehensive set of physical parameters. The dimensionless group containing the drag force is found to be $F_D/\rho U^2 L^2$, where L is a length scale, and U is the freestream velocity. This suggests that the drag coefficient is naturally defined as $C_D = F_D/\rho U^2 L^2$, however it is customary to define the drag coefficient instead as

$$C_D = \frac{F_D}{\frac{1}{2} \rho U^2 A} \quad (14.22a)$$

where the area A normally refers to the frontal area of the object, and the factor of $\frac{1}{2}$ is introduced to produce a denominator that is the product of the dynamic pressure of the upstream flow $\frac{1}{2} \rho U^2$ times the frontal area. (In defining the drag coefficient for a wing, the area is said to be the planform area, i.e., the area of the wing as seen from above.) The DA further shows that the drag coefficient may be written as

$$C_D = C_D \left(Re, M, Fr, St, We, \frac{e}{L} \right) \quad (14.22b)$$

which shows that the drag coefficient for an object of a given shape may depend on Reynolds number, Mach number, Froude number, Strouhal number, Weber number, and dimensionless groups. In some cases the drag coefficient may even depend on additional depend on a dimensionless rotation group. From your study of DA, you know that the mere presence of a group in Eq. 14.22b does not mean that all groups are equally important. For example, it is difficult to see how the effect of surface tension, which is characterized by the value of the Weber number, would be significant in engineering applications involving ships and other large objects moving on or through an air-water interface. On the other hand, if we were asked to estimate the drag experienced by a water strider or other aquatic insect, the effect of surface tension would likely be quite important. In the next four sections we present empirical results for the drag coefficient, beginning with low Reynolds number flows.

CD/Dynamics/Low Reynolds number flows

14.4.1 Low Reynolds Number Flow

Low Reynolds number flows of engineering interest include creeping flows, for which $Re \ll 1$, as well as flows in which the Reynolds number is not large enough for a distinct boundary layer to be observed. The Reynolds number range over which the boundary layer is indistinct might be roughly estimated as $0.1 < Re < 100$. In low Reynolds number flows involving air and water, the Reynolds number is usually small because the

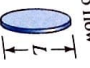
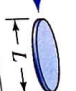
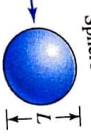

Object	Circular disk normal to flow 	Circular disk parallel to flow 	Sphere 	Hemisphere 
$C_D = \frac{F_D}{\frac{1}{2}\rho U^2 \left(\frac{\pi L^2}{4}\right)}$ (for $Re \leq 1$)	20.4/ Re	13.6/ Re	24.0/ Re	22.2/ Re

Figure 14.17 Drag coefficients for creeping flow. ($Re = UL/\nu \ll 1$).

length scale of the object is small. Viscous effects in low Reynolds number flows are not confined near the body surface, and both friction and form drag contribute to the total drag. Drag coefficients derived from analytical solutions can be found for many objects of simple shape in creeping flows. Experimental data for slightly larger Reynolds numbers can also be found for cylinders and spheres. If analytical or experimental results are not available for the shape of interest, it is also possible to use computational fluid dynamics to determine the flow over an object in both creeping flow and at slightly larger Reynolds numbers. The drag coefficient can then be calculated directly from the solution.

Drag coefficients are shown in Figure 14.17 for a several shapes in creeping flow. The dependence of these drag coefficients on the inverse of the fluid density, are negligible in creeping flows. This means that a dimensional analysis applicable only to creeping flow would not include density; rather, it would assume $F_D = f(L, U, \mu)$, where L is the length scale defining a particular smooth object. Choosing L as a repeating parameter leads to $F_D/\mu UL = C$, where C is a constant. This correctly indicates that a drag coefficient for creeping flow should not contain density. However, since $F_D = C\mu UL$, forming the drag coefficient in the customary way gives

$$C_D = \frac{F_D}{\frac{1}{2}\rho U^2 L^2} = C \frac{\mu UL}{\frac{1}{2}\rho U^2 L^2} = \frac{2C}{Re}$$

We see that all objects in creeping flow have drag coefficients that are proportional to Re^{-1} . Note carefully, however, that this decrease in drag coefficient with increasing Reynolds number applies only to creeping flow, $Re \ll 1$, not to larger Reynolds numbers. The drag on an object in a creeping flow increases linearly with velocity.

EXAMPLE 14.3

A playful child left alone has run a vacuum cleaner in reverse, creating a dust cloud. If the cloud consists of 0.001, 0.01, and 0.1 mm diameter particles, and the particle density is 700 kg/m^3 , will the child be able to clean up the mess by dusting the furniture before her mother returns an hour later? Assume that the particles near the ceiling must settle 2.5 m before depositing on various surfaces, and that the air temperature is 20°C .

SOLUTION

For a particle settling at terminal velocity, a vertical force balance shows that

$$W = F_{\text{air}}$$

where $W = \rho_p g V$ is the weight of a particle of density ρ_p , and F_{air} is the total force applied by the air to the particle. The force applied by the air consists of a drag force F_D that accounts for the relative motion of the particle through the stationary air and a buoyancy force F_B that accounts for the effects of the hydrostatic pressure variation in the air. Because the buoyancy force is not included when the drag force is calculated by using a drag coefficient, we must write

$$W = F_D + F_B \quad (\text{A})$$

(Another way to think about this problem is revealed by rearranging this equation as $W - F_B = F_D$. Since $W - F_B$ is the weight of the particle as measured in air, we see that the force balance equates this weight, which causes the particle to settle, to the drag force that resists the settling motion.) Substituting for each term in the force balance (A) gives

$$\rho_p g V = C_D \frac{1}{2} \rho_{\text{air}} U^2 A + \rho_{\text{air}} g V$$

Solving for the terminal velocity we obtain

$$U = \sqrt{\frac{2(\rho_p - \rho_{\text{air}})gV}{C_D \rho_{\text{air}} A}} \quad (\text{B})$$

We will assume a spherical particle and a creeping flow drag coefficient given by $C_D = 24/Re$. Note that since $C_D = 24/Re = 24\mu/(\rho_{\text{air}} U D)$ in this case, the terminal velocity also occurs in the drag coefficient in (B). The area and volume are $A = \pi D^2/4$ and $V = \pi D^3/6$, respectively; hence $V/A = 2D/3$. Inserting these values into (B) shows that the terminal velocity is given by

$$U = \frac{(\rho_p - \rho_{\text{air}})gD^2}{18\mu} \quad (\text{C})$$

The time needed for a particle to settle from a height H is $t = H/U$. Thus the settling time is

$$t = \frac{18\mu H}{(\rho_p - \rho_{\text{air}})gD^2} \quad (\text{D})$$

Since the diameter occurs in the denominator, the smallest particles take the longest time to settle. The maximum settling time t_{max} is found using $H = 2.5 \text{ m}$. Inserting data for air $\rho_{\text{air}} = 1.2 \text{ kg/m}^3$, $\mu = 1.81 \times 10^{-5} \text{ (N}\cdot\text{s)/m}^2$, and other values into (B)–(D), we can construct the following table showing t_{max} for each particle size:

D (mm)	U (m/s)	t_{max} (minutes)	Re
0.001	2.1×10^{-5}	2000	1.4×10^{-6}
0.01	2.1×10^{-3}	20	1.4×10^{-3}
0.1	2.1×10^{-1}	0.2	1.4

The calculated Reynolds numbers confirm the validity of the creeping flow assumption. It is evident that the smallest particles, which take ~ 33 h to settle, will pose a problem. Note that since $\rho_{\text{air}} = 0.7\% \rho_P$, buoyancy is negligible in this example.



CD/Video library/Flow past a cylinder

14.4.2 Cylinders



Figure 14.18 provides drag coefficient data for a smooth cylinder over a large range of Reynolds number. The frontal area of the cylinder enters the drag coefficient as $A = DL$, where D is the diameter of the cylinder and L its length. Although the data in Figure 14.18 apply only in principle to a cylinder of infinite length, the information is used to estimate the drag on finite length cylinders. The error made will increase as the aspect ratio L/D decreases. In applications for which $L/D < 4$, it is better to use the drag coefficient given later (Section 14.4.4, Table 14.2).

Examination of Figure 14.18 shows that the drag coefficient is a complex function of Reynolds number. To understand the influence of Re on C_D , consider Figure 14.19, a flow visualization of the velocity profiles on a cylinder. As you follow the flow around the cylinder, notice that the laminar boundary layer velocity profile is gradually deformed until the flow reverses direction. The corresponding pressure distributions, both the inviscid approximation and the empirically observed distribution, are shown in

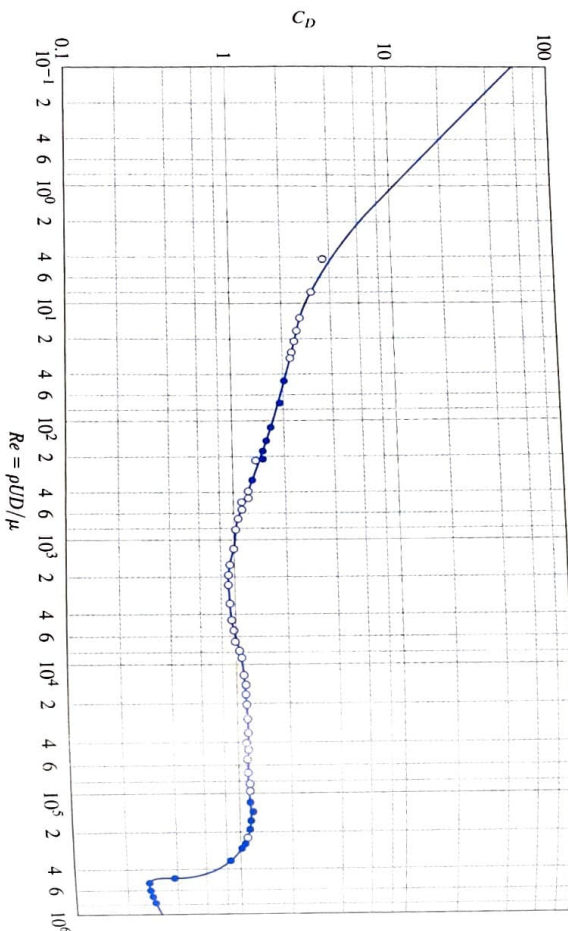


Figure 14.18 Drag coefficient for a smooth cylinder.



Figure 14.19 Flow visualization of the boundary layer on a cylinder created with hydrogen bubbles.

The visual aspects of the flow field over a cylinder are a strong function of the Reynolds number. Consider the obvious difference in the flows illustrated in Figures 12.2 and 12.3. In the creeping flow uses 12.2 ($Re = 0.038$), there is no wake behind the cylinder. However, in Figure 12.3 ($Re = 19$), a wake has formed because flow separation has occurred even though there is no boundary layer present. At much larger Reynolds numbers the size of the wake is determined by boundary layer separation, and as noted earlier, this influences the pressure drag.

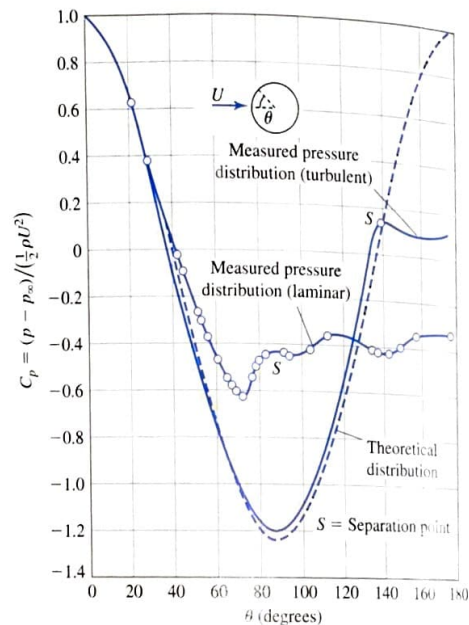
is, the pressure drag in the inviscid model is identically zero. That can be seen that the actual pressure recovery is much less than that for the inviscid flow case. Thus, for the real viscous flow we find a net force retarding the motion of the cylinder. This is the source of the pressure drag (or form drag) on a cylinder.

We are now in a position to explain the dependence of C_D on Re for a cylinder, as illustrated in Figure 14.18. In the low Reynolds number regime, the drag coefficient is proportional to the inverse of Reynolds number as already explained. For $1 < Re < 10^3$ the friction drag of the laminar boundary layer tends to dominate the form drag, so C_D varies with Re in much the same way that it did for laminar flow over an aligned flat plate (i.e., $C_D \propto Re^{-1/2}$). In the range $10^3 < Re < 10^5$, C_D has only a weak dependence on Re and the total drag is dominated by the pressure or form drag. This behavior is similar to that displayed by "bluff bodies," as described later (Section 14.4.4).

Over the range $10^5 < Re < 10^6$ the cylinder drag coefficient falls dramatically by about 80%. At this critical point the drag actually decreases with increasing speed. Imagine increasing the speed of your car while letting up on the gas. What accounts for this extraordinary behavior? You might attribute it to the laminar-to-turbulent transition of the boundary layer. Recall Figure 14.8, which shows laminar and turbulent flow profiles. The higher velocity and momentum flux near the surface for turbulent flow causes an increase of friction drag, but results in a substantial decrease in pressure drag. How is this possible? Well, remember that the boundary layer separates when the streamwise momentum of the flow is insufficient to overcome the adverse pressure

Figure 14.20. Focus your attention on the true pressure distribution and note that as the fluid in the boundary layer moves from the front of the cylinder to the top, it is accelerated by a favorable pressure gradient. However, as the fluid passes the top, the pressure gradient becomes unfavorable, tending to slow the fluid down. As long as the fluid has enough momentum, it can still move forward, but viscous effects and the pressure gradient tend to exert a decelerating effect. Eventually all the forward momentum is dissipated and the flow reverses direction (see Figure 14.19). This is the phenomenon that was evident in the Falkner-Skan solution discussed earlier.

Figure 14.20 Comparison of the pressure distribution around a cylinder based on inviscid theory and empirical observations.



EXAMPLE 14.4

A modern sculpture includes a wind gage in the form of a circular cylinder suspended from two fine wires as shown in Figure 14.21. If the presence of the wires is assumed to have a negligible influence on the flow field, at what angle will the cylinder hang in a wind of 25 km/h? The cylinder weighs 6 N and its dimensions are $D = 10$ cm and $L = 1$ m.

SOLUTION

Since the wind applies a lift and drag to the cylinder, after neglecting the tiny buoyancy force on the cylinder, and writing a force balance on the cylinder in the x and y directions we obtain

$$(F_D \cos \theta + F_L \sin \theta) - W \sin \theta = 0 \quad \text{and} \quad 2T - W \cos \theta + (F_L \cos \theta - F_D \sin \theta) = 0$$

Noting that the x component of force of the wind ($F_D \cos \theta + F_L \sin \theta$) = $C_D \frac{1}{2} \rho_{\text{air}} (U \cos \theta)^2 A$, the force balance in the x direction shows that

$$\sin \theta = \frac{(C_D \frac{1}{2} \rho_{\text{air}} U^2 A) (\cos^2 \theta)}{W} \quad (\text{A})$$

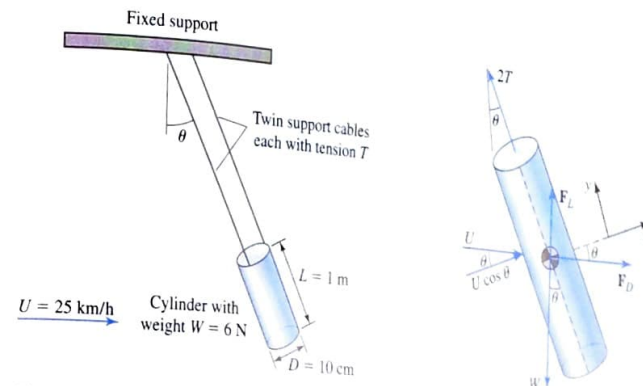


Figure 14.21 Schematic for Example 14.4.

We expect that the angle will be larger for a lighter cylinder at any given wind speed but can never exceed 90° . For small angles, $\cos^2 \theta \approx 1$, and since $A = DL$, we obtain the approximate result

$$\theta = \sin^{-1} \left(\frac{C_D \rho_{\text{air}} U^2 DL}{2W} \right) \quad (\text{B})$$

Assuming 20°C air for which $\rho = 1.2 \text{ kg/m}^3$ and $\nu = 1.51 \times 10^{-5} \text{ m}^2/\text{s}$, the Reynolds number is

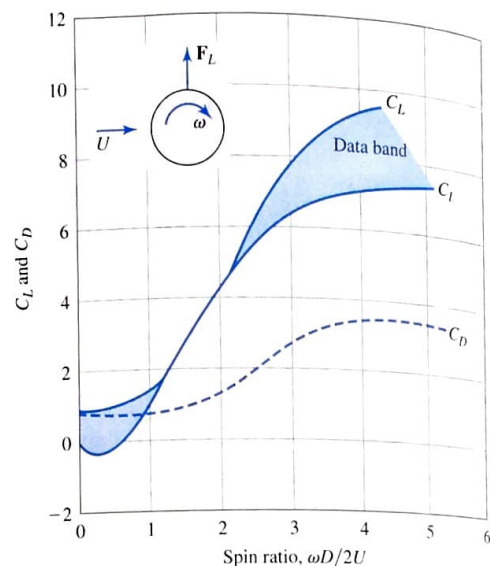
$$Re = \frac{UD}{\nu} = \frac{(25 \text{ km/h})(1000 \text{ m/km})(h/3600 \text{ s})(0.1 \text{ m})}{1.51 \times 10^{-5} \text{ m}^2/\text{s}} = 4.6 \times 10^4$$

From Figure 14.18, at this Reynolds number $C_D = 1.2$. Inserting the data into (A) we must iterate or use a symbolic code to solve

$$\sin \theta = \left[\frac{(1.2)(1.2 \text{ kg/m}^3)[(25 \text{ km/h})(1000 \text{ m/km})(h/3600 \text{ s})]^2 (0.1 \text{ m})(1 \text{ m})}{2(6 \text{ N})} \right] \cos^2 \theta$$

The result is $\theta = 27.2^\circ$. It is easy to confirm that (B) does not deliver good accuracy in this case. Depending on the range of wind speeds expected at the sculpture site, it may be best to employ a lighter cylinder to obtain a larger angle of deflection. We should also be aware that the aspect ratio of the cylinder affects the drag coefficient so it may be best to validate a design based on (A) or (B) by careful calibration experiments.

Figure 14.22 Lift and drag coefficients for a spinning cylinder.



gradient. The increased momentum in the boundary layer in turbulent flow causes separation to be delayed, and the resulting wake is smaller. The pressure on the downstream side of the cylinder is therefore not quite as low as it is with a large wake, and the result is a much lower form drag. This is evident in the changed pressure distribution on the cylinder surface as shown in Figure 14.20.

Spinning a cylinder in a freestream results in an increase in drag if the rotation rate is sufficiently large. The rotation also creates a side force or lift on the cylinder. This is known as the Magnus effect. The lift and drag coefficients for a spinning cylinder are shown in Figure 14.22. In this case the lift coefficient is defined as $C_L = F_L / \frac{1}{2} \rho U^2 DL$. Over the years a number of interesting uses for spinning cylinders have been proposed, including a rotor-based wind-powered ship (Figure 14.23).

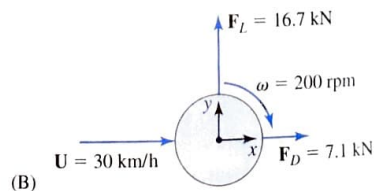


Figure 14.23 (A) The *Bruckau*, designed by Anton Flettner. (B) Schematic for Example 14.5.

EXAMPLE 14.5

The Flettner rotor-powered ship shown in Figure 14.23A had two rotors, each 3 m diameter and 15 m tall. If $\omega = 200$ rpm and the speed of the wind relative to the rotor is 30 km/h, find the force applied to each rotor by the wind.

SOLUTION

To find the force generated by each rotor, we will use the results for a spinning cylinder as shown in Figure 14.22 to determine the lift and drag coefficients. First we calculate the rotational velocity as

$$V_\theta = R\omega = (0.0015 \text{ km})(200 \text{ rpm})(2\pi \text{ rad/rev})(60 \text{ min/h}) = 113 \text{ km/h}$$

Dividing this value by the wind speed gives us the spin ratio $WD/2U$. Thus we have

$$\frac{V_\theta}{U} = \frac{113 \text{ km/h}}{30 \text{ km/h}} = 3.75$$

From Figure 14.22 we find $C_L = 8.9$ and $C_D = 3.8$. Thus the lift and drag forces are

$$F_L = C_L \frac{1}{2} \rho U^2 DL = (8.9) \left(\frac{1}{2} \right) (1.2 \text{ kg/m}^3) (8.33 \text{ m/s})^2 (3 \text{ m})(15 \text{ m}) = 16.7 \text{ kN}$$

$$F_D = C_D \frac{1}{2} \rho U^2 DL = (3.8) \left(\frac{1}{2} \right) (1.2 \text{ kg/m}^3) (8.33 \text{ m/s})^2 (3 \text{ m})(15 \text{ m}) = 7.1 \text{ kN}$$

where we have assumed air at 20°C in calculating the density. The force applied by the wind to each rotor is thus given by $\mathbf{F}_{\text{wind}} = 7.1 \text{ kN} \mathbf{i} + 16.7 \text{ kN} \mathbf{j}$ as shown in Figure 14.23B. This force acts at an angle of $\theta = \tan^{-1}(16.7/7.1) = 67^\circ$ to the left of the relative wind direction.

CD/Video library/Flow past a sphere

14.4.3 Spheres



Figure 14.24 shows drag coefficient data for a smooth sphere over a broad range of Re . The frontal area of the sphere enters the drag coefficient as $A = \pi D^2/4$. Spheres exhibit drag coefficient behavior with Reynolds number that is similar to that of cylinders, for much the same reasons. The change in separation point due to the transition from a laminar to turbulent boundary layer is evident in Figure 14.25.

It is interesting to note that golf balls in flight have Reynolds numbers near the point at which the laminar-to-turbulent boundary layer transition occurs. To ensure that the boundary layer is turbulent, roughness is added to the surface of the ball in the form of dimples. These dimples reduce flow separation, thereby lowering the drag and increasing the flight distance. The effect of roughness on C_D for spheres near the turbulent transition is shown in Figure 14.26.

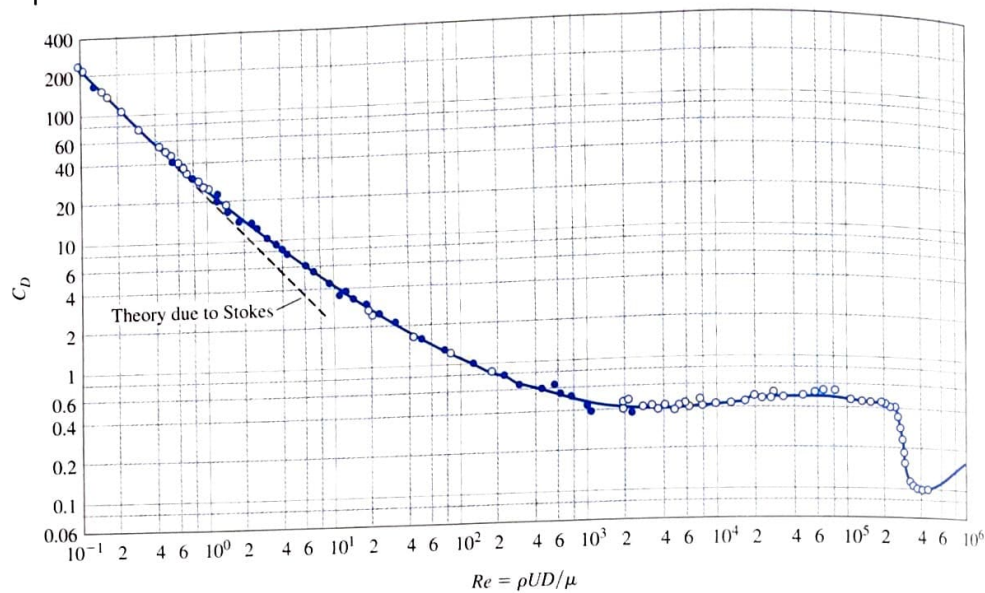


Figure 14.24 Drag coefficient for a smooth sphere.

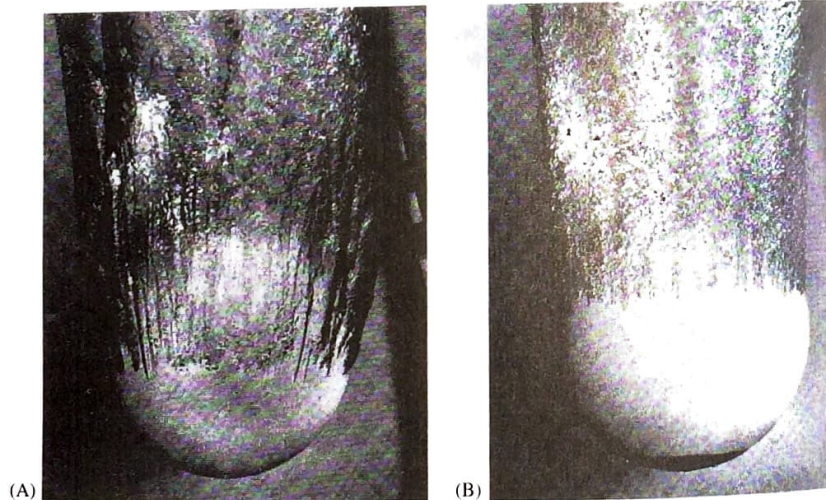


Figure 14.25 Boundary layer separation on a sphere for (A) laminar flow and (B) turbulent flow caused by roughing the nose.

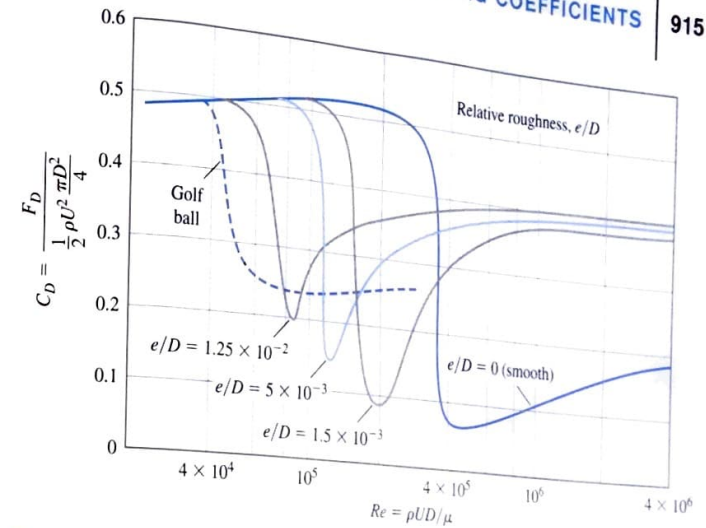


Figure 14.26 The effect of roughness on the drag on a sphere.

EXAMPLE 14.6

To make a car easier to find in crowded parking lots, a colorful 2 in. diameter smooth plastic ball is attached to the end of the vehicle's 3 ft antenna as shown in Figure 14.27. What is the bending moment on the antenna due to the ball if the car is moving at 50 mph?

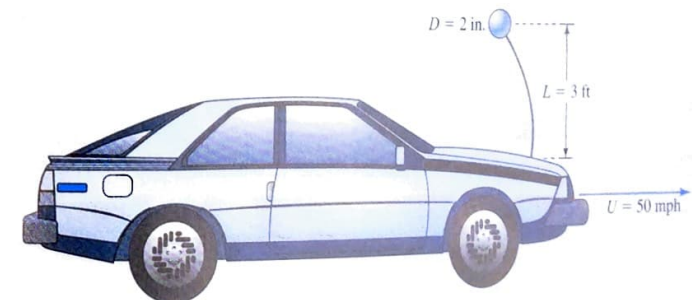


Figure 14.27 Schematic for Example 14.6.

SOLUTION

We will calculate the drag force on the ball, then find the resulting bending moment. We will assume that the flow over the ball is the same as it would be without having the

antenna nearby. Assuming air at 70°F,

$$Re = \frac{UD}{\nu} = \frac{(50 \text{ mph})[1.47 \text{ ft}/(\text{mph}\cdot\text{s})](2 \text{ in.})(\text{ft}/12 \text{ in.})}{1.64 \times 10^{-4} \text{ ft}^2/\text{s}} = 7.5 \times 10^4$$

From Figure 14.24 we find $C_D = 0.5$. The drag force on the ball is calculated next from $F_D = C_D \frac{1}{2} \rho U^2 A$, where $A = \pi D^2/4$. Inserting the data, we find

$$F_D = (0.5) \left(\frac{1}{2} \right) (2.329 \times 10^{-3} \text{ slug}/\text{ft}^3) (73.3 \text{ ft/s})^2 \frac{\pi (0.1667 \text{ ft})^2}{4} \\ = 6.83 \times 10^{-2} \text{ lb}_f$$

Ignoring any curvature of the antenna, the bending moment is

$$M = F_D L = (6.83 \times 10^{-2} \text{ lb}_f)(3 \text{ ft}) = 0.2 \text{ ft}\cdot\text{lb}_f$$

Would you recommend adding roughness to the ball?



CD/Boundary layers/Separation

No discussion of the external flow over a sphere would be complete without including the effect of rotation, which plays a prominent role in the flight of sport balls of all types. As was the case with a cylinder, rotation of a sphere not only affects the drag but also produces a sideforce or lift. The lift and drag coefficients for rotating spheres are shown in Figure 14.28. The lift coefficient for a sphere is defined by $C_L = F_L / \frac{1}{2} \rho U^2 A$, where $A = \pi D^2/4$.

14.4.4 Bluff Bodies

Suppose you were asked what feature buildings, billboards, and beams have in common that might strongly affect their drag? If you recognized that each of these objects has a relatively flat face with sharp edges, you are correct. These and other nonstreamlined objects are called bluff bodies. More formally, “bluff body” refers to an object that experiences flow separation at a relatively low Reynolds number and has a flow field after separation occurs that is relatively unchanged as Re increases. As a result, the drag coefficient for a bluff body after separation is nearly independent of Reynolds number (over a large range of Re). The separation process on a bluff body is often, but not always, associated with a sharp corner or other change in geometry.

From our discussions, you know that the onset of flow separation generally corresponds to an increase in total drag resulting from a substantial increase in the form drag, and that form drag can be reduced by streamlining. Consider the tractor trailer truck

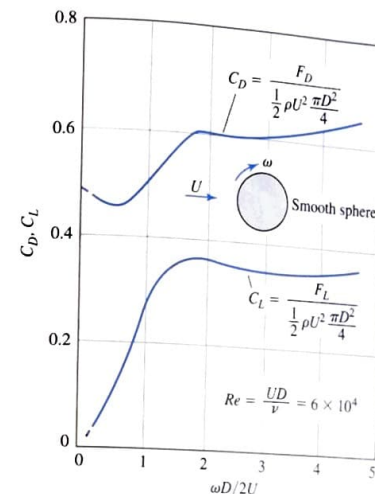


Figure 14.28 Lift and drag coefficients for a spinning sphere.

EXAMPLE 14.7

A baseball pitcher throws his curve ball at 80 mph with a rotational speed of 1800 rpm. The ball has a mass of 5 oz and a 9 in. circumference. Estimate how much this pitch will break as it travels a distance of 55 ft in a spring game in New York, when the air temperature is 50°F. What is the break in a summer game when the temperature is 90°F? In your calculation, assume that the rotation axis of the ball is vertical.

SOLUTION

In the coordinates shown in Figure 14.29, the rotation of the ball will cause a force tending to move the ball in the y direction. The equation of motion for the ball in the y direction of break is $Ma_y = \sum F_y$. The drag on the ball acts in the x direction and tends to slow the ball down slightly during its travel to the plate. We will neglect this effect and assume for the ball a constant velocity of 80 mph. The time of flight of the ball is therefore given by

$$T = \frac{S}{V_{\text{ball}}} \quad (\text{A})$$

where S is the distance to the plate and V_{ball} is the speed of the ball. Inserting the data, we calculate a flight time

$$T = \frac{S}{V_{\text{ball}}} = \left(\frac{55 \text{ ft}}{80 \text{ mph}} \right) \left(\frac{1 \text{ mph}}{1.467 \text{ ft/s}} \right) = 0.47 \text{ s}$$

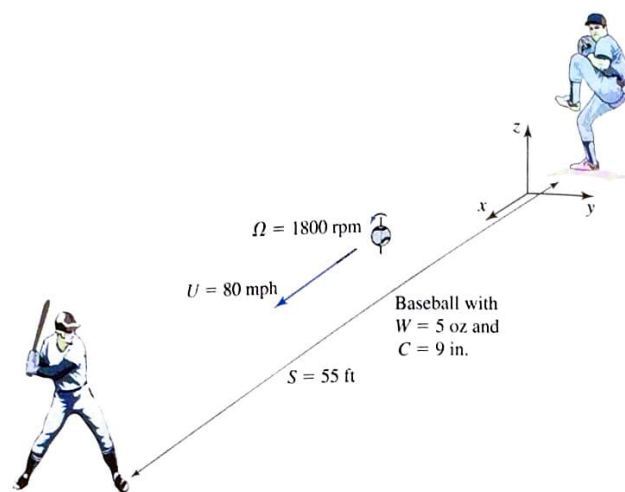


Figure 14.29 Schematic for Example 14.7.

Gravity acts on the ball in the negative z direction and causes the ball to drop as it travels to the plate. We will assume this effect acts independently of the lift force created by the rotation of the ball; hence the drop can be calculated as approximately 2.9 ft. The lift force for a rotating smooth sphere is given by

$$F_L = \frac{1}{2} \rho V_{\text{ball}}^2 \frac{\pi D^2}{4} C_L \quad (\text{B})$$

and acts in the y direction. A baseball has raised stitches that are known to affect the trajectory of a pitch. Since we have lift and drag data only for a smooth sphere as given in Figure 14.29, we will use the smooth sphere data in our calculation. Finally, note that if the rotational speed of the ball is assumed constant, then the lift force is constant during the flight.

We can write the equation of motion for the ball in the y direction as $m a_y = m(d^2 y/dt^2) = F_L$. Integrating this twice we obtain $y(t) = (F_L/m)(t^2/2) + C_0 t + C_1$. To evaluate the constants, note that at time $t = 0$, the ball is at an initial location y_0 , thus $C_1 = y_0$, and we can write $y(t) - y_0 = (F_L/m)(t^2/2) + C_0 t$. The remaining constant is found by assuming that the ball has no velocity component in the y direction when released by the pitcher. This allows us to set $C_0 = 0$ and obtain $y(t) - y_0 = (F_L/m)(t^2/2)$. At time T the break or distance traveled in the y direction is given by

$$\Delta y = \frac{F_L}{m} \frac{T^2}{2} \quad (\text{C})$$

Inserting (A) and (B) we have

$$\Delta y = \frac{\pi D^2 \rho C_L S^2}{16m} \quad (\text{D})$$

To determine the lift coefficient, we first calculate the speed ratio

$$\frac{U}{V_{\text{ball}}} = \frac{D\omega}{2V_{\text{ball}}} = \frac{(2.865 \text{ in.})(\text{ft}/12 \text{ in.})(1800 \text{ rpm})(2\pi)(60 \text{ min/h})}{2(80 \text{ mph})(5280 \text{ ft/mile})} = 0.19$$

then use the chart in Figure 14.28 to find that $C_L \approx 0.05$. To calculate the break at the different air temperatures, note that $\rho_{50} = 2.420 \times 10^{-3} \text{ slug/ft}^3$, and $\rho_{90} = 2.244 \times 10^{-3} \text{ slug/ft}^3$. The diameter of the ball is found to be $D = (9 \text{ in.}/\pi)(1 \text{ ft}/12 \text{ in.}) = 0.2387 \text{ ft}$. Thus from (D) we find the break at 50°F is

$$\begin{aligned} \Delta y_{50} &= \frac{\pi D^2 \rho C_L S^2}{16m} \\ \Delta y_{50} &= \left(\frac{\pi}{16}\right) \left(\frac{1}{5 \text{ oz}}\right) \left(\frac{1 \text{ oz}}{1.943 \times 10^{-3} \text{ slug}}\right) (0.2387 \text{ ft})^2 (2.420 \times 10^{-3} \text{ slug/ft}^3) (0.05) (55 \text{ ft})^2 \\ \Delta y_{50} &= 0.42 \text{ ft} \end{aligned}$$

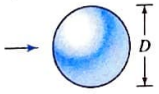

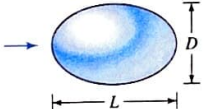

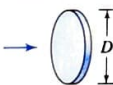
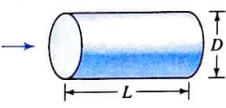
At 90°F the break is

$$\begin{aligned} \Delta y_{90} &= \left(\frac{\rho_{90}}{\rho_{50}}\right) \Delta y_{50} = \left(\frac{2.244 \times 10^{-3} \text{ slug/ft}^3}{2.420 \times 10^{-3} \text{ slug/ft}^3}\right) 0.42 \text{ ft} \\ &= 0.39 \text{ ft} \end{aligned}$$

or about 8% less in the "lighter" summer air. This break is not sufficient to fool a batter if the curve ball is thrown with the rotation axis vertical, as indicated in Figure 14.29. Instead the pitcher throws the ball so that the break is down, i.e., the rotation axis is nearly horizontal. Pitchers use a variety of spins to induce movement of the ball. A knuckle ball is thrown with no spin and darts erratically owing to flow separation. A discussion of the physics of sports balls can be found in an article by R. D. Mehta entitled "Aerodynamics of Sports Balls," in *Annual Review of Fluid Mechanics*, volume 17, pages 151–189, 1985.

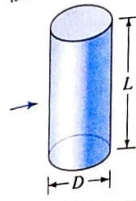
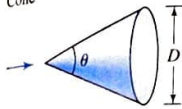
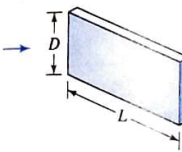
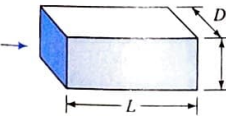

shown in Figure 14.30A. The large flat section of the trailer exposed to the air above the cab is a good example of a bluff body (the cab itself is somewhat streamlined); as such, it causes substantial drag, which reduces gas mileage. Figure 14.30B shows a similar rig with a wind deflector mounted on the roof of the cab in front of the bluff body. This simple and inexpensive streamlining device substantially reduces the drag on the trailer and,

TABLE 14.2 Drag Coefficients for selected 3D objects.

Geometry	Reference Area, A	Drag Coefficient, C_D , and Remarks																		
<p>Sphere</p> 	$\frac{\pi D^2}{4}$	<table><tr><th>Re</th><th>10^2</th><th>10^3</th><th>10^4</th><th>10^5</th><th>10^6</th><th>5×10^6</th></tr><tr><td>C_D</td><td>1.0</td><td>0.41</td><td>0.39</td><td>0.52</td><td>0.12</td><td>0.18</td></tr></table> <p>For $Re < 1$, $C_D \approx 24/[Re\{1 + (3/16)Re\}]$.</p>	Re	10^2	10^3	10^4	10^5	10^6	5×10^6	C_D	1.0	0.41	0.39	0.52	0.12	0.18				
Re	10^2	10^3	10^4	10^5	10^6	5×10^6														
C_D	1.0	0.41	0.39	0.52	0.12	0.18														
<p>Hemisphere</p> 	$\frac{\pi D^2}{4}$	<p>$C_D = 0.42$ (Sphere side facing upstream)</p> <p>$C_D = 1.17$ (Flat side facing upstream)</p>																		
<p>Ellipsoid of Revolution</p> 	$\frac{\pi D^2}{4}$	<p>$C_D = 0.44(D/L) + 0.016(L/D) + 0.016(D/L)^{1/2}$</p> <p>$1 < L/D < 10$.</p> <p>$Re < 2 \times 10^5$, laminar flow.</p>																		
<p>Sphere in a Circular Duct</p> 	$\frac{\pi D^2}{4}$	<p>$C_D = \left[1 + 1.45 \left(\frac{D}{D_0}\right)^{4.5}\right] C_{D D_0/D=\infty}$</p> <p>$0 < D/D_0 < 0.92$, $C_{D D_0/D=\infty}$ is that of sphere above.</p>																		
<p>Thin Circular Disk</p> 	$\frac{\pi D^2}{4}$	<table><tr><th>Re</th><th>1</th><th>2</th><th>5</th><th>10</th><th>10^2</th><th>10^3</th><th>10^4</th><th>10^5</th></tr><tr><td>C_D</td><td>25</td><td>15</td><td>6</td><td>3.6</td><td>1.5</td><td>1.1</td><td>1.1</td><td>1.15</td></tr></table>	Re	1	2	5	10	10^2	10^3	10^4	10^5	C_D	25	15	6	3.6	1.5	1.1	1.1	1.15
Re	1	2	5	10	10^2	10^3	10^4	10^5												
C_D	25	15	6	3.6	1.5	1.1	1.1	1.15												
<p>Circular Rod Parallel to Flow</p> 	$\frac{\pi D^2}{4}$	<table><tr><th>L/D</th><th>C_D</th></tr><tr><td>~ 0</td><td>1.15</td></tr><tr><td>0.5</td><td>1.10</td></tr><tr><td>1.0</td><td>0.93</td></tr><tr><td>1.5</td><td>0.85</td></tr><tr><td>2.0</td><td>0.83</td></tr><tr><td>3.0</td><td>0.85</td></tr><tr><td>4.0</td><td>0.85</td></tr><tr><td>5.0</td><td>0.85</td></tr></table> <p>$Re \geq 10^4$</p>	L/D	C_D	~ 0	1.15	0.5	1.10	1.0	0.93	1.5	0.85	2.0	0.83	3.0	0.85	4.0	0.85	5.0	0.85
L/D	C_D																			
~ 0	1.15																			
0.5	1.10																			
1.0	0.93																			
1.5	0.85																			
2.0	0.83																			
3.0	0.85																			
4.0	0.85																			
5.0	0.85																			

(continued)

TABLE 14.2 (continued)

Geometry	Reference Area, A	Drag Coefficient, C_D , and Remarks																				
<p>Cylindrical Rod Perpendicular to Flow</p> 	LD	<table><tr><th>L/D</th><th>C_D</th></tr><tr><td>1.0</td><td>0.64</td></tr><tr><td>1.98</td><td>0.68</td></tr><tr><td>2.96</td><td>0.74</td></tr><tr><td>5.0</td><td>0.74</td></tr><tr><td>10.</td><td>0.82</td></tr><tr><td>20.</td><td>0.91</td></tr><tr><td>40.</td><td>0.98</td></tr><tr><td>∞</td><td>1.20</td></tr></table> <p>$Re \geq 10^4$</p>	L/D	C_D	1.0	0.64	1.98	0.68	2.96	0.74	5.0	0.74	10.	0.82	20.	0.91	40.	0.98	∞	1.20		
L/D	C_D																					
1.0	0.64																					
1.98	0.68																					
2.96	0.74																					
5.0	0.74																					
10.	0.82																					
20.	0.91																					
40.	0.98																					
∞	1.20																					
<p>Cone</p> 	$\frac{\pi D^2}{4}$	<table><tr><th>θ (deg)</th><th>C_D</th></tr><tr><td>10</td><td>0.30</td></tr><tr><td>20</td><td>0.40</td></tr><tr><td>30</td><td>0.55</td></tr><tr><td>40</td><td>0.65</td></tr><tr><td>60</td><td>0.80</td></tr><tr><td>75</td><td>1.05</td></tr><tr><td>90</td><td>1.15</td></tr><tr><td>180</td><td>1.40</td></tr></table> <p>$Re \geq 10^4$</p>	θ (deg)	C_D	10	0.30	20	0.40	30	0.55	40	0.65	60	0.80	75	1.05	90	1.15	180	1.40		
θ (deg)	C_D																					
10	0.30																					
20	0.40																					
30	0.55																					
40	0.65																					
60	0.80																					
75	1.05																					
90	1.15																					
180	1.40																					
<p>Thin Rectangular Plate Perpendicular to Flow</p> 	LD	<table><tr><th>L/D</th><th>C_D</th></tr><tr><td>1.0</td><td>1.05</td></tr><tr><td>2.0</td><td>1.10</td></tr><tr><td>4.0</td><td>1.12</td></tr><tr><td>8.0</td><td>1.20</td></tr><tr><td>10.0</td><td>1.22</td></tr><tr><td>12.0</td><td>1.22</td></tr><tr><td>17.8</td><td>1.33</td></tr><tr><td>∞</td><td>1.90</td></tr></table> <p>$Re \geq 10^4$</p>	L/D	C_D	1.0	1.05	2.0	1.10	4.0	1.12	8.0	1.20	10.0	1.22	12.0	1.22	17.8	1.33	∞	1.90		
L/D	C_D																					
1.0	1.05																					
2.0	1.10																					
4.0	1.12																					
8.0	1.20																					
10.0	1.22																					
12.0	1.22																					
17.8	1.33																					
∞	1.90																					
<p>Square Rod Parallel to Flow</p> 	D^2	<table><tr><th>L/D</th><th>C_D</th></tr><tr><td>~ 0</td><td>1.25</td></tr><tr><td>0.5</td><td>1.25</td></tr><tr><td>1.0</td><td>1.15</td></tr><tr><td>1.5</td><td>0.97</td></tr><tr><td>2.0</td><td>0.87</td></tr><tr><td>2.5</td><td>0.90</td></tr><tr><td>3.0</td><td>0.93</td></tr><tr><td>4.0</td><td>0.95</td></tr><tr><td>5.0</td><td>0.95</td></tr></table> <p>$Re \geq 10^4$</p>	L/D	C_D	~ 0	1.25	0.5	1.25	1.0	1.15	1.5	0.97	2.0	0.87	2.5	0.90	3.0	0.93	4.0	0.95	5.0	0.95
L/D	C_D																					
~ 0	1.25																					
0.5	1.25																					
1.0	1.15																					
1.5	0.97																					
2.0	0.87																					
2.5	0.90																					
3.0	0.93																					
4.0	0.95																					
5.0	0.95																					
<p>Average Man</p> 	<p>See data at right. For $C_D A$ product appropriate to different flow directions and posture.</p>	<p>→ $C_D A = 9 \text{ ft}^2$ (0.84 m^2) ↑ $C_D A = 1.2 \text{ ft}^2$ (0.11 m^2) • $C_D A = 5 \text{ ft}^2$ (0.46 m^2) Sitting → $C_D A = 6 \text{ ft}^2$ (0.56 m^2) Crouching → $C_D A = 2$ to 3 ft^2 (0.19 m^2 to 0.28 m^2)</p>																				

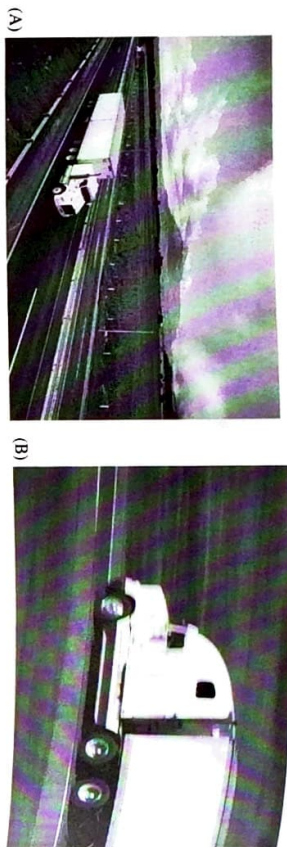


Figure 14.30 (A) Bluff body truck design. (B) Streamlined truck design.

therefore, increases fuel economy. A person riding a bicycle is another example of a bluff body. Have you noticed that riders in the Tour de France generally wear helmets designed to provide a more streamlined shape and reduce pressure drag?

Table 14.2 includes drag coefficients for a few common bluff bodies as adapted from a variety of sources. The data are for $Re > 10^4$ with accuracy of $\pm 5\%$. The interested reader is referred to *Applied Fluid Dynamics Handbook*, by Robert Blevins for a more complete listing of drag coefficients for bluff bodies. Notice that, as expected,

EXAMPLE 14.8

As shown schematically in Figure 14.31, square columns 4 in. \times 4 in. and 10 ft tall are to be used in the construction of a porch in south Florida. If the columns are exposed to hurricane force winds of 100 mph ($= 147$ ft/s), what force must each column withstand?

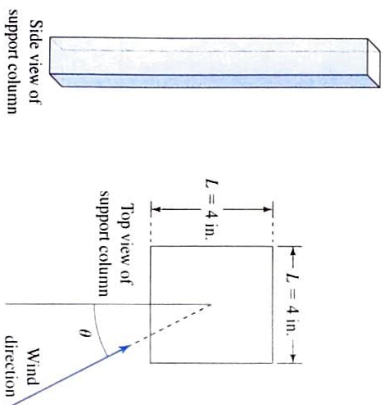


Figure 14.31 Schematic for Example 14.8.

SOLUTION

The Reynolds number of the flow is found to be

$$Re = \frac{UD}{\nu} = \frac{(147 \text{ ft/s})(4 \text{ in.})(ft/12 \text{ in.})}{1.64 \times 10^{-4} \text{ ft}^2/\text{s}} = 3 \times 10^5$$

which is above the value $Re > 10^4$ for which the data for a square section in Table 14.3 are valid. Thus it is appropriate to use the drag coefficient in this table for our analysis. In Table 14.3 we see that for a square section, the maximum $C_D = 2.4$ is at 45° to the wind, thus the maximum force will occur for a wind that comes from this direction. This is the force the column must potentially withstand in the worst case. To calculate it, we will assume 70°F air and use $A = (4/12 \text{ ft})(10 \text{ ft}) = 3.33 \text{ ft}^2$ and $U = 147 \text{ ft/s}$. The drag force is then found to be

$$F_D = \frac{1}{2} \rho U^2 A C_D = \frac{1}{2} (2.329 \times 10^{-3} \text{ slug/ft}^3) [147 \text{ ft/s}]^2 (3.33 \text{ ft}^2) (2.4) = 200 \text{ lbf}$$

the reported C_D values for sharp edged bluff bodies are either independent of, or only a weak function of, Re over the range indicated.

Table 14.3 provides similar data for 2D bluff sections. A bluff section is defined to be the (constant) cross section of an object that has infinite depth. The C_D for the sections is based on force per unit span. The reported drag coefficients are also for $Re > 10^4$ with accuracy of $\pm 5\%$.

You may have noticed that the outside mirrors on modern automobiles are highly streamlined in appearance, and noticeably different in shape from the disk-shaped mirrors seen on early automobiles. Door handles on automobiles have also undergone changes over the years and are now almost always flush with the surface of the door rather than projecting. Mirrors and door handles on automobiles are examples of protrances, objects that are partly immersed in a freestream and capable of creating a considerable amount of drag. The streamlining of mirrors and door handles reflects a concern for fuel economy, as does the overall lowering of drag coefficients on vehicles of all types. The effect of a protrance is enhanced if the nearby flow has been accelerated to a high speed by the shape of the body to which the protrance is attached. Thus if a protrance is necessary to the function of a vehicle or device, it is wise to locate it in a region of retarded airflow rather than where the airflow is moving at or above the freestream value. In the early days of automotive design, windshield wipers on many models moved from the top of the windshield to the base, then were tucked under the hood, getting them completely out of the airflow.

CD/Boundary layers/Separation/Airfoil separation

CD/Dynamics/Dependence of forces on Reynolds number and geometry/Effect of Re and geometry on flow

TABLE 14.3 Drag Coefficients for selected 2D sections.

Geometry	Drag Coefficient, C_D , and Remarks						
	Re	10^2	10^3	10^4	10^5	10^6	10^7
Circular Cylinder	C_D	1.4	1.0	1.1	1.2	0.4	0.8
	For $Re < 1$, $C_D \approx 8\pi/[Re \log_e (7.4/Re)]$.						
Cylinder Near a Wall	E/D	0	0.8	0.6	0.25	0.15	0.05
	C_D	0.25	1.1	1.2	0.15	0.05	0.02
	C_L	0	0.6	0.25	0.15	0.05	0.02
	E/D	0.25	1.1	1.2	0.15	0.05	0.02
	C_D	1.0	1.3	0.05	0.02	0	0
	C_L	1.5	1.2	0	0	0	0
	E/D	2.0	1.2	0	0	0	0
	C_D	4.0	1.2	0	0	0	0
Cylinder Downstream of Another Cylinder	$T/D = 0$						
	C_D	1.0	1.1	1.0	0.65	0.65	0.65
Drag on Downstream Cylinder	$T/D = 1.0$						
	C_D	1.0	1.1	1.0	0.65	0.65	0.65
	$T/D = 2$						
	C_D	1.0	1.1	1.0	0.65	0.65	0.65
	$T/D = 4.0$						
	C_D	1.0	1.1	1.0	0.65	0.65	0.65
	$T/D = 10^4$						
	C_D	1.0	1.1	1.0	0.65	0.65	0.65

$10^4 < Re < 10^5$
Lift force is away from wall.

TABLE 14.3 (continued)

Geometry	Drag Coefficient, C_D , and Remarks						
	E/D	C_D	C_L	C_D	C_L	C_D	C_L
Two Cylinders Side by Side	0	1.6	0.8	0.25	1.0	0.6	0.4
	0.25	1.0	0.6	0.5	0.9	0.4	0.2
	1.0	1.1	0.2	1.5	1.3	0.1	0.1
	2.0	1.2	0.05	4.0	1.2	0.05	0.0
	4.0	1.2	0.0	6.0	1.2	0.0	0.0
	1.2	0.0	0.0	1.2	0.0	0.0	0.0
	1.2	0.0	0.0	1.2	0.0	0.0	0.0
	1.2	0.0	0.0	1.2	0.0	0.0	0.0
Inclined Square	θ (Deg)	0	5	10	15	20	25
	C_D	2.2	2.1	1.8	1.3	1.9	2.1
Rounded Nose Section	L/D	0.5	1.16	1.0	0.90	2.0	0.70
	C_D	2.0	0.70	4.0	0.68	6.0	0.64

C_D, C_L for each cylinder. $10^4 < Re < 10^5$. Lift force is repulsive.

θ (Deg) 0 5 10 15 20 25 30 35 40 45
 C_D 2.2 2.1 1.8 1.3 1.9 2.1 2.2 2.3 2.4 2.4
 $Re \geq 10^4$

Geometry	Drag Coefficient, C_D , and Remarks						
	Re	10^2	10^3	10^4	10^5	10^6	10^7
Circular Cylinder	C_D	1.4	1.0	1.1	1.2	0.4	0.8
	For $Re < 1$, $C_D \approx 8\pi/[Re \log_e (7.4/Re)]$.						
Cylinder Near a Wall	E/D	0	0.8	0.6	0.25	0.15	0.05
	C_D	0.25	1.1	1.2	0.15	0.05	0.02
	C_L	0	0.6	0.25	0.15	0.05	0.02
	E/D	0.25	1.1	1.2	0.15	0.05	0.02
	C_D	1.0	1.3	0.05	0.02	0	0
	C_L	1.5	1.2	0	0	0	0
	E/D	2.0	1.2	0	0	0	0
	C_D	4.0	1.2	0	0	0	0
Cylinder Downstream of Another Cylinder	$T/D = 0$						
	C_D	1.0	1.1	1.0	0.65	0.65	0.65
Drag on Downstream Cylinder	$T/D = 1.0$						
	C_D	1.0	1.1	1.0	0.65	0.65	0.65
	$T/D = 2$						
	C_D	1.0	1.1	1.0	0.65	0.65	0.65
	$T/D = 4.0$						
	C_D	1.0	1.1	1.0	0.65	0.65	0.65
	$T/D = 10^4$						
	C_D	1.0	1.1	1.0	0.65	0.65	0.65
Rectangle	L/D	0.1	1.9	1.0	2.2	2.1	2.1
	C_D	0.2	2.1	1.2	1.5	1.8	1.6
Thin Plate Extending from a Wall	D/L	0.125	0.3	0.6	1.0	1.0	1.0
	C_D	0.25	0.3	0.6	1.0	1.0	1.0
	D/L	0.50	0.6	1.0	1.0	1.0	1.0
	C_D	1.0	1.0	1.0	1.0	1.0	1.0
	D/L	2.0	1.6	2.5	1.4	1.3	1.3
	C_D	3.0	1.4	2.5	1.4	1.3	1.3
	D/L	3.0	1.3	2.5	1.4	1.3	1.3
	C_D	6.0	0.89	2.5	1.4	1.3	1.3

$Re \geq 10^4$

Geometry	Drag Coefficient, C_D , and Remarks						
	Re	10^2	10^3	10^4	10^5	10^6	10^7
Circular Cylinder	C_D	1.4	1.0	1.1	1.2	0.4	0.8
	For $Re < 1$, $C_D \approx 8\pi/[Re \log_e (7.4/Re)]$.						
Cylinder Near a Wall	E/D	0	0.8	0.6	0.25	0.15	0.05
	C_D	0.25	1.1	1.2	0.15	0.05	0.02
	C_L	0	0.6	0.25	0.15	0.05	0.02
	E/D	0.25	1.1	1.2	0.15	0.05	0.02
	C_D	1.0	1.3	0.05	0.02	0	0
	C_L	1.5	1.2	0	0	0	0
	E/D	2.0	1.2	0	0	0	0
	C_D	4.0	1.2	0	0	0	0
Cylinder Downstream of Another Cylinder	$T/D = 0$						
	C_D	1.0	1.1	1.0	0.65	0.65	0.65
Drag on Downstream Cylinder	$T/D = 1.0$						
	C_D	1.0	1.1	1.0	0.65	0.65	0.65
	$T/D = 2$						
	C_D	1.0	1.1	1.0	0.65	0.65	0.65
	$T/D = 4.0$						
	C_D	1.0	1.1	1.0	0.65	0.65	0.65
	$T/D = 10^4$						
	C_D	1.0	1.1	1.0	0.65	0.65	0.65
Rectangle	L/D	0.1	1.9	1.0	2.2	2.1	2.1
	C_D	0.2	2.1	1.2	1.5	1.8	1.6
Thin Plate Extending from a Wall	D/L	0.125	0.3	0.6	1.0	1.0	1.0
	C_D	0.25	0.3	0.6	1.0	1.0	1.0
	D/L	0.50	0.6	1.0	1.0	1.0	1.0
	C_D	1.0	1.0	1.0	1.0	1.0	1.0
	D/L	2.0	1.6	2.5	1.4	1.3	1.3
	C_D	3.0	1.4	2.5	1.4	1.3	1.3
	D/L	3.0	1.3	2.5	1.4	1.3	1.3
	C_D	6.0	0.89	2.5	1.4	1.3	1.3

$Re \geq 10^4$

Geometry	Drag Coefficient, C_D , and Remarks						
	Re	10^2	10^3	10^4	10^5	10^6	10^7
Circular Cylinder	C_D	1.4	1.0	1.1	1.2	0.4	0.8
	For $Re < 1$, $C_D \approx 8\pi/[Re \log_e (7.4/Re)]$.						
Cylinder Near a Wall	E/D	0	0.8	0.6	0.25	0.15	0.05
	C_D	0.25	1.1	1.2	0.15	0.05	0.02
	C_L	0	0.6	0.25	0.15	0.05	0.02
	E/D	0.25	1.1	1.2	0.15	0.05	0.02
	C_D	1.0	1.3	0.05	0.02	0	0
	C_L	1.5	1.2	0	0	0	0
	E/D	2.0	1.2	0	0	0	0
	C_D	4.0	1.2	0	0	0	0
Cylinder Downstream of Another Cylinder	$T/D = 0$						
	C_D	1.0	1.1	1.0	0.65	0.65	0.65
Drag on Downstream Cylinder	$T/D = 1.0$						
	C_D	1.0	1.1	1.0	0.65	0.65	0.65
	$T/D = 2$						
	C_D	1.0	1.1	1.0	0.65	0.65	0.65
	$T/D = 4.0$						
	C_D	1.0	1.1	1.0	0.65	0.65	0.65
	$T/D = 10^4$						
	C_D	1.0	1.1	1.0	0.65	0.65	0.65
Rectangle	L/D	0.1	1.9	1.0	2.2	2.1	2.1
	C_D	0.2	2.1	1.2	1.5	1.8	1.6
Thin Plate Extending from a Wall	D/L	0.125	0.3	0.6	1.0	1.0	1.0
	C_D	0.25	0.3	0.6	1.0	1.0	1.0
	D/L	0.50	0.6	1.0	1.0	1.0	1.0
	C_D	1.0	1.0	1.0	1.0	1.0	1.0
	D/L	2.0	1.6	2.5	1.4	1.3	1.3
	C_D	3.0	1.4	2.5	1.4	1.3	1.3
	D/L	3.0	1.3	2.5	1.4	1.3	1.3
	C_D	6.0	0.89	2.5	1.4	1.3	1.3

$Re \geq 10^4$

Rounded Nose Section

L/D	C_D	
0.5	1.16	
1.0	0.90	
2.0	0.70	$Re \geq 10^4$
4.0	0.68	
6.0	0.64	

Thin Flat Plate Inclined to Flow

$$T < 0.1D$$

$$C_N \approx \begin{cases} \frac{2\pi \tan \theta / \theta < 8^\circ}{0.222 + 0.283 / \sin \theta} & 90^\circ \geq \theta > 12^\circ \\ & Re \geq 10^4 \end{cases}$$

$$C_L = C_N \cos \theta$$

$$C_D = C_N \sin \theta$$

There is a discontinuity in the range $8^\circ < \theta < 12^\circ$ with $C_N \approx 0.8$ as flow separates from upper surface. See Table 14.2 for $\theta = 0^\circ$.

Thin Plate Extending from a Wall

$$C_D = 1.4$$

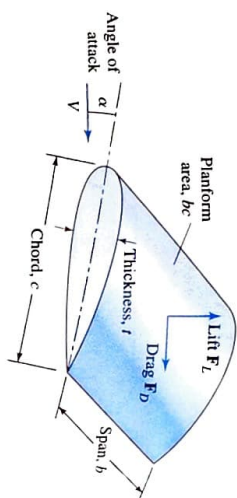
$$Re \geq 10^4$$

Ellipse

$$D/L \quad C_D$$

$$0.125 \quad 0.22$$

Figure 14.34 Airfoil geometry.



Applying dimensional analysis leads to the following relationships among dimensionless groups:

$$\frac{F_L}{\frac{1}{2}\rho V^2 bc} = g_1 \left(Re_c, \frac{t}{c}, \alpha \right) \quad \text{and} \quad \frac{F_D}{\frac{1}{2}\rho V^2 bc} = g_2 \left(Re_c, \frac{t}{c}, \alpha \right)$$

where Re_c is the Reynolds number based on chord length.

The lift and drag coefficients for an airfoil section are defined by Eqs. 3.43 as

$$C_L = \frac{F_L}{\frac{1}{2}\rho V^2 bc} \quad \text{and} \quad C_D = \frac{F_D}{\frac{1}{2}\rho V^2 bc}$$

where the product bc is called the platform area. Thus we conclude that the dependence of the lift and drag coefficients on the various dimensionless groups is given by

$$C_L = C_L \left[Re_c, \frac{t}{c}, \alpha \right] \quad \text{and} \quad C_D = C_D \left[Re_c, \frac{t}{c}, \alpha \right]$$

For an infinitely long wing, the span does not enter the analysis, so the ratio of span to chord, b/c , disappears from these expressions. We conclude that the lift and drag coefficients are a function of Reynolds number, the geometry of the airfoil as expressed by the ratio of thickness to chord, and the angle of attack. For engineering purposes, empirical data for a given airfoil shape are presented in the form of lift and drag coefficients as a function of angle of attack for an infinitely long wing of the indicated shape. An example of lift and drag data as a function of angle of attack for the symmetric airfoil NACA 0018 is provided in Figure 14.35. Note that for this symmetric airfoil the lift is zero at zero angle of attack ($\alpha = 0$).

A comparison of the NACA 0018 airfoil shape (Figure 14.35) and the NACA 23012 airfoil shape (Figure 14.36) shows that while the centerline of the former is straight, the centerline of the latter is curved. An airfoil with a curved centerline is said to be cambered. Camber provides lift at zero angle of attack by making the flow field around the airfoil nonsymmetrical. Fluid moving over the top of a cambered airfoil at zero angle of

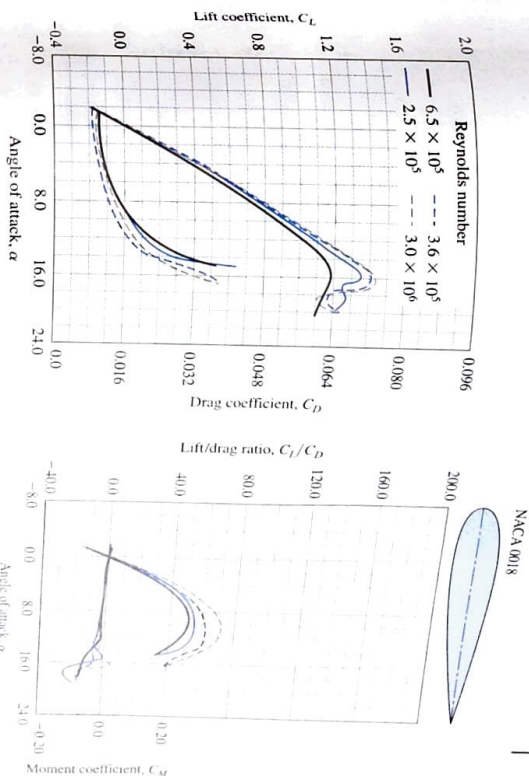


Figure 14.35 Lift and drag coefficients for the NACA 0018 airfoil. 3D test on smooth surface, 2% turbulence.

attack is moving at a higher velocity than the fluid along the bottom. Thus, Bernoulli's equation tells us that the pressure on top is lower than the pressure on the bottom. As always, an unequal pressure distribution is the source of lift. Lift and drag coefficient data as a function of angle of attack for the cambered airfoil section NACA 23012 are shown in Figure 14.36.

From the foregoing discussion it should be clear that high speed air must be flowing over the top of an airfoil for it to produce lift. As the angle of attack of any airfoil increases, the separation point moves forward from the rear of the airfoil. Eventually, if the angle of attack becomes too great, a separation bubble will cover nearly the whole top of the airfoil. This phenomenon, called stall, results in a loss of lift. The onset of stall can be viewed in the series of flow visualizations in Figure 14.37. Figures 14.37c at $\alpha = 30^\circ$ and Figure 14.37d at $\alpha = 30^\circ$ indicate the abrupt onset of stall. An aircraft will literally fall out of the sky if the wings stall.

Aircraft wings must operate in several different modes. For example, in level flight minimized drag with maximized lift is desired. During landing, however, drag is beneficial in slowing the plane down. Thus, no single wing or airfoil shape can be optimized for all the operational modes. A solution to this problem lies in making the wing adjustable. Flaps, on both the leading and trailing edges, change the airfoil shape, i.e., they can alter the amount of camber. Figure 14.38a shows an airfoil at a high angle of attack

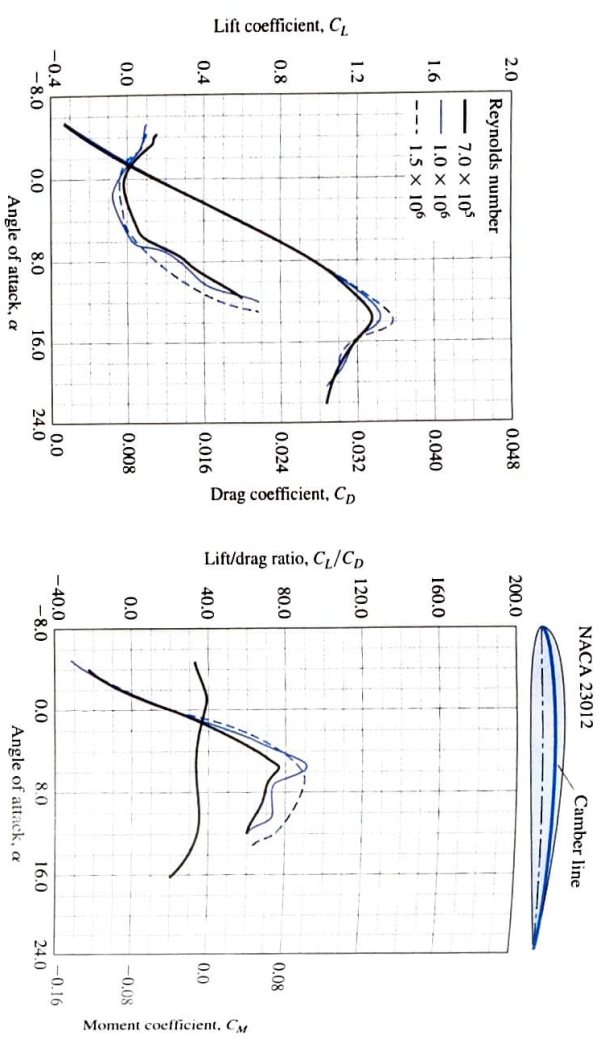


Figure 14.36 Lift and drag coefficients for the NACA 23012 airfoil: 2D test in tunnel on smooth surface at 0.02% turbulence.

with flaps extended in a landing configuration. Figure 14.38B shows the cruise and take-off configurations in comparison to the landing configuration.

If you look closely at Figure 14.38A you can see slots between the flaps that allow air from the lower surface to flow to the top, helping to delay flow separation. This is only one of the sophisticated methods of boundary layer control that have been developed. Figure 14.39 shows the upper surface of a wing of a commercial aircraft. Note the array of protuberances on the wing surface. We know they will increase the friction drag. However, by causing high momentum air to flow into the boundary layer, these vortex generators keep the boundary layer attached longer, reducing pressure drag and/or delaying the onset of stall.

So far, our discussion of the flow over an airfoil has been limited to 2D flow, such as would occur if a wing were of infinite length. Real wings of finite length have greater drag than is predicted by 2D airfoil theory. The increase in drag is called induced drag. One cause is the leakage of high pressure air on the bottom of the wing to the low pressure upper side around the wing tip. Figure 14.40 shows a flow visualization of the wing tip vortices that are generated as a result of this phenomenon.

The next time you are in an airplane, the view from your window should be much more interesting because you will be able to appreciate the complex physics of the air-flow and the sophisticated design of the wing.

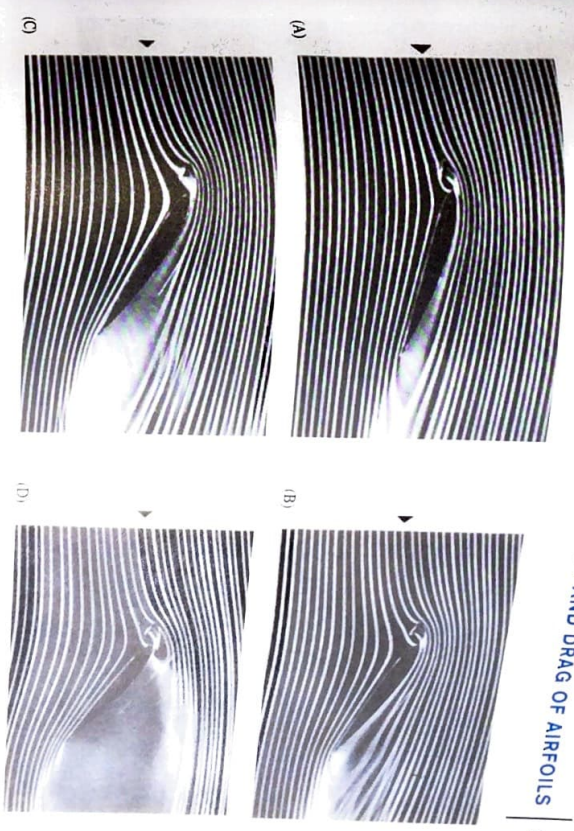


Figure 14.37 NACA 4412 airfoil section with a leading edge flap that delays flow separation from about 15 to 30°.

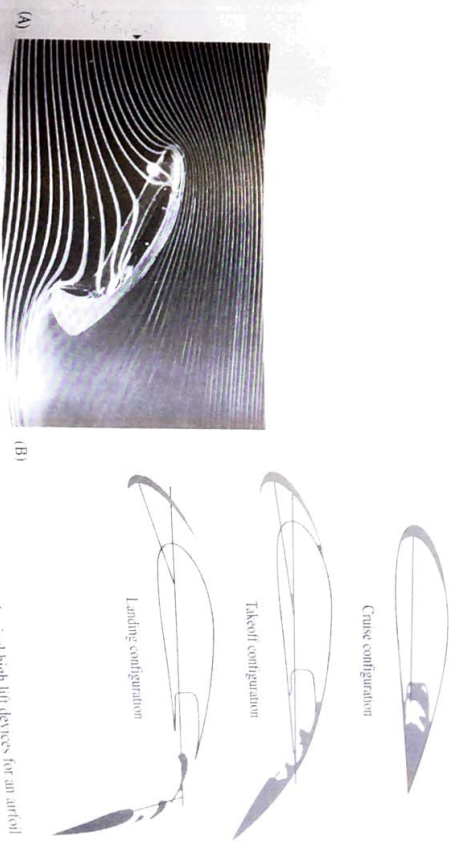


Figure 14.38 (A) Airfoil section at a 25° angle of attack. (B) Sophisticated mechanical high lift devices for an airfoil section.



Figure 14.39 Vortex generators on a commercial aircraft.



Figure 14.40 Wing tip vortex.

EXAMPLE 14.9

A fully loaded aircraft weighing 900 kN has a wing area of 230 m^2 . If the wing has the characteristics of a NACA 23012 airfoil and during takeoff operates at a 6° angle of attack, what is the required takeoff speed at sea level? What is the takeoff speed at an elevation of 2000 m?

SOLUTION

To take off, the lift force must overcome the weight, so $F_L = W$,

$$\frac{1}{2} \rho U^2 A C_L = W$$

$$U = \sqrt{\frac{2W}{\rho A C_L}}$$

From Appendix B for the U.S. Standard Atmosphere $\rho(0 \text{ m}) = 1.225 \text{ kg/m}^3$ and $\rho(2000 \text{ m}) = 1.007 \text{ kg/m}^3$. From Figure 14.36 $C_L = 0.79$. Substituting the data into

the preceding expression yields:

$$U = \sqrt{\frac{2(900 \times 10^3 \text{ N})}{(1.225 \text{ kg/m}^3)(230 \text{ m}^2)(0.79)}} = 90 \text{ m/s} = 324 \text{ km/h}$$

at sea level and at 2000 m

$$U = \sqrt{\frac{2(900 \times 10^3 \text{ N})}{(1.007 \text{ kg/m}^3)(230 \text{ m}^2)(0.79)}} = 99 \text{ m/s} = 356 \text{ km/h}$$

Thus an increase of almost 10% in takeoff speed is required at the higher elevation.

14.6 SUMMARY

"External flow" is the term used to describe either an object moving through a fluid or fluid moving over an object. The study of external flows is important in a wide variety of fields including transportation (lift and drag) and structural design (fluid forces).

When a body is immersed in a moving fluid, the fluid velocity along a line perpendicular to any point on its surface is observed to vary from zero on the surface to a maximum value some distance away. At large Re the variation occurs over a relatively small distance, and the body is said to have a boundary layer. The boundary layer characteristics are affected by several factors, including the shape of the surface and its orientation relative to the freestream.

The Blasius solution applies to the steady, laminar boundary layer on a smooth flat plate aligned with the freestream and yields the following important results: (1) the pressure inside the boundary layer is the same as it is in the inviscid flow outside the boundary layer; (2) the boundary layer thickness grows at a rate $\delta(x) \propto x^{1/2}$; and (3) the wall shear stress and skin friction coefficient decreases at a rate $\tau_w(x) \propto x^{-1/2}$. The quantitative results from the Blasius solution are provided in Eqs. 14.12a–14.12h. Since it is observed that the transition to turbulence occurs at $Re_x \approx 5 \times 10^5$ for a flat plate, the Blasius solution is valid for $0 < x < 5 \times 10^5 (v/U)$.

There is no analytical solution for a turbulent boundary layer on a flat plate; so we are forced to rely on empirical observations. The results of the corresponding power-law model are given in Eqs. 14.16a–14.16h and are valid for the range $5 \times 10^5 < Re_x < 10^7$. The boundary layer thickness grows at a rate proportional to $x^{4/5}$, while the wall shear stress and skin friction coefficient decreases at a rate proportional to $x^{-1/5}$.

Observation of boundary layers on airfoils and other curved bodies show that an object's shape and angle of attack have a significant effect on the characteristics of both laminar and turbulent boundary layers. For a boundary layer, the effects of shape and angle of attack are equivalent to a streamwise pressure gradient. A pressure gradient of the form $dp/dx < 0$, meaning that the pressure is decreasing (and the fluid is accelerating) in the flow direction, is referred to as a favorable pressure gradient, while

$dp/dx > 0$ is termed an unfavorable pressure gradient. The favorable pressure gradient of an accelerating freestream tends to thin a laminar boundary layer and bring higher momentum fluid nearer the surface, while the unfavorable pressure gradient of a decelerating freestream tends to do the opposite. Thus, on an airfoil a laminar boundary layer is relatively thin and remains attached on portions of the surface where the flow is accelerating, but becomes thicker and may separate from portions of the surface where the flow is decelerating. At the point of separation the wall shear stress is zero, and downstream of this point the flow near the wall reverses direction. This also occurs with turbulent boundary layers, although they are more resistant to flow separation owing to the increased amount of higher momentum fluid near the surface associated with the more blunt turbulent velocity profile.

For a stationary object immersed in a moving stream, drag is the component of force exerted on the object by the fluid in the direction of the freestream. For an object moving through a stationary fluid, the drag acts in the direction opposite to the object's motion. The power required to propel an object through a fluid at constant speed is given by the product of the drag and the speed. Thus, drag limits the performance of vehicles of all types and affects their fuel economy. The total drag force arises from two mechanisms: pressure and shear stress. The pressure contribution to the total drag is referred to as form drag, and the contribution due to the shear stress acting on an object's surface is called friction drag. In a high Re flows the drag on bluff bodies tends to be dominated by form drag. The drag on long thin bodies tends to be dominated by skin friction. "Streamlining" is a term used to describe the attempt to design an optimum shape for a bluff body in a high Re flow by minimizing the total drag. It generally takes the form of elongating the rear of the body. Although this raises the friction drag, it lowers the form drag, and the total drag is reduced.

Although CFD is increasingly being used to determine the drag on objects of engineering interest, much of what is known about drag is the result of experiments. Dimensional analysis shows that the drag coefficient may depend on Re , M , Fr , St , We , and ϵ/D . Drag coefficients are shown in Figure 14.17 for a number of shapes in creeping flow. All objects in creeping flow have drag coefficients that are proportional to Re^{-1} . Figure 14.18 provides C_D data for a smooth cylinder. For $Re < 10^3$ the friction drag of the laminar boundary layer dominates, so C_D varies with Re as it did for laminar flow over an aligned flat plate (i.e., $C_D \propto Re^{-1/2}$). In the range $10^3 < Re < 10^5$, C_D has only a weak dependence on Re and the total drag is dominated by pressure drag. Over the range $10^5 < Re < 10^6$, C_D falls dramatically by about 80%. The drag actually decreases with increasing speed as a result of the laminar-to-turbulent transition of the boundary layer. Spinning a cylinder can result in an increase in drag and also creates a sideforce or lift on the cylinder. Figure 14.24 provides C_D data for a smooth sphere. The trends for the dependence of C_D on Re for a sphere are similar to those for a cylinder, for many of the same reasons. As was the case with a cylinder, rotation of a sphere not only affects the drag but also produces lift.

The term "bluff body" refers to an object that experiences flow separation at a relatively low Re and for which the point of separation is essentially independent of Re . The fixed point of separation is often, but not always, associated with a sharp corner or change in geometry. Since the flow separation point is independent of Re , the drag coefficients for a bluff body is also nearly independent of Reynolds number (over a large range of Re). Tables 14.2 gives the relevant geometry, characteristic area, and drag coefficients for a few common bluff bodies.

Airfoils are designed to maximize lift while minimizing drag. The lift on an airfoil is primarily due to the pressure distribution. In contrast, the drag of an airfoil depends on both the pressure and shear stress distributions. An airfoil shape may be thought of as the end result of streamlining an otherwise bluff body. The trade-off in adding material to shapes are presented in the form of lift and drag coefficients, as a function of angle of attack.

PROBLEMS

Section 14.2

14.1 Assuming that the wing on an airplane is behaving like a flat plate, what is the length of the laminar boundary layer if it is flying at a speed 150 mph at an altitude of 5000 ft.

14.2 Calculate δ , δ^* , and θ for the boundary layer flow described in Problem 14.1.

14.3 Air, at 20°C, with incoming velocity of $U = 18$ m/s, flows over a horizontal flat plate. The velocity profile in the boundary layer is modeled by

$$\frac{u}{U} = \sin\left(\frac{\pi y}{2\delta}\right) + C$$

where C is a constant. At $x = 0.15$ m the boundary layer thickness is $\delta = 5.0$ mm. What are the boundary conditions that this

Calculate the moment flux for each profile

and the turbulent profile is the $1/7$ -power law equation

$$\frac{u}{U} = \left(\frac{y}{\delta}\right)^{1/7}$$

profile must satisfy? What is the value of C ? Is the boundary layer laminar or turbulent at this point? Why?

14.4 Determine δ^* , θ , and τ_w at $x = 0.15$ m for the flow described in Problem 14.3.

14.5 The laminar and turbulent velocity profiles in Figure P14.1 have the same boundary layer thickness. The laminar profile is parabolic

$$\frac{u}{U} = 2\left(\frac{y}{\delta}\right) - \left(\frac{y}{\delta}\right)^2$$

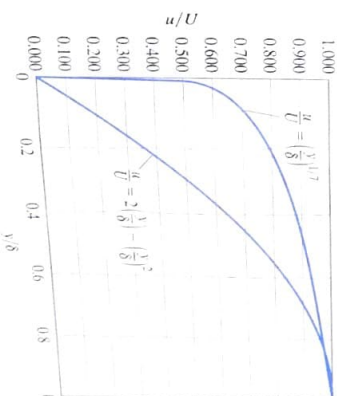


Figure P14.1